

Transparent and Breathable Ion Gel-Based Sensors toward Multimodal Sensing Ability

Yuji Isano, Hajime Fujita, Koki Murakami, Sijie Ni, Yuta Kurotaki, Tamami Takano, Yutaka Isoda, Ryosuke Matsuda, Fumika Nakamura, Yuuki Nishitai, Nyamjargal Ochirkhuyag, Kota Inoue, Hiroki Kawakami, Yusuke Okubo, Kazuhide Ueno, Toshinori Fujie, and Hiroki Ota*

Polymer thin-film sensors have attracted considerable attention in various applications owing to their highly transparent, flexible, and gas-permeable features. However, conventional thin-film sensors based on nanomaterials suffer from poor selectivity in sensing targets and scalability of functions. Therefore, a new approach is required for achieving higher selectivity with simple processibility. This study proposes highly transparent, ultra-flexible, and gas-permeable polymer thin-film sensors using ion gels as the sensing material; the sensors demonstrated the capacity for selective detections. Particularly, this study demonstrates simultaneous and independent sensing of temperature and humidity as a proof of concept. The sensors are fabricated using a simple spray coating method on a thin silicone rubber film ($\approx 25 \mu\text{m}$ thickness). Owing to their thin-film shape, the sensors exhibit more than 80% visible light transmittance and a higher gas permeability than the human transepidermal water loss. The temperature and humidity are simultaneously detected with a high sensitivity of $15.4\% \text{ } ^\circ\text{C}^{-1}$ and 2.0% per percentage of the relative humidity, respectively, using gels containing two different ionic liquids (ILs). The results suggest that the easily modifiable nature of ILs enables the fabrication of ultra-flexible and transparent sensors that can detect various objects using a simple method.

film sensors have been developed. These sensors are required to be ultra-flexible to ensure adhesion to curved planar surfaces,^[1] such as biological surfaces, and transparent to perform their functions without compromising the appearance of the introduced object. Temperature,^[2] humidity,^[3] strain,^[4] and pressure^[5,6] sensors have been developed as such transparent and ultra-flexible thin-film sensors. Polymer materials are used as substrates in these sensors. Nanocarbon materials, such as carbon nanotubes (CNTs), graphene, metal nanowires, and conductive polymers are used as electrodes.^[7] CNTs and graphene are used not only as electrode materials, but also as sensing materials.^[8] The sensors fabricated using these materials are expected to be introduced in displays,^[9] for the measurement of deformations in the human face,^[7] and for breathing rate detection.^[10]

In addition to transparency and ultra-flexibility, high gas permeability has been identified as a requisite sensor property in recent years. This is because the primary application of these sensors is in wearable devices for living organisms^[11,12] and plants,^[13,14] and long-term use and comfort are important for practical implementation. The use of sensors having low

1. Introduction

With the development of Internet of Things (IoT) technology, which can obtain information on any environment, various thin-

Y. Isano, K. Murakami, S. Ni, Y. Kurotaki, T. Takano, Y. Isoda, R. Matsuda, F. Nakamura, Y. Nishitai, N. Ochirkhuyag, K. Inoue, H. Kawakami, H. Ota

Department of Mechanical Engineering
Yokohama National University
79-5, Tokiwadai, Hodogaya-ku, Yokohama, Kanagawa 240–8501, Japan
E-mail: ota-hiroki-xm@ynu.ac.jp

H. Fujita, T. Fujie
School of Life Science and Technology
Tokyo Institute of Technology
4259 Nagatsuta-cho, Midori-ku, Yokohama, Kanagawa 226–8501, Japan

Y. Okubo
Division of Cellular and Molecular Toxicology
Biological Safety and Research Center
National Institute of Health Sciences
3-25-26 Tonomachi, Kawasaki-ku, Kawasaki, Kanagawa 210–9501, Japan

K. Ueno
Department of Chemistry and Life Science
Yokohama National University
79-5 Tokiwadai, Hodogaya-ku, Yokohama 240–8501, Japan

K. Ueno
Center for Advanced Chemical Energy Research Center
Institute of Advanced Sciences
Yokohama National University
79-5 Tokiwadai, Hodogaya-ku, Yokohama 240–8501, Japan

H. Ota
Graduate School of System Integration
Yokohama National University
79-5, Tokiwadai, Hodogaya-ku, Yokohama, Kanagawa 240–8501, Japan

 The ORCID identification number(s) for the author(s) of this article can be found under <https://doi.org/10.1002/admt.202200209>.

DOI: 10.1002/admt.202200209

gas permeability on the skin can cause discomfort and dermatitis, because of the retention of the moisture that evaporates from the skin between the sensor and the skin.^[15] To solve this problem, sensors using a nanomesh^[16] or polymer ultrathin film^[17] as the substrate were developed.

To achieve the three characteristics of transparency, flexibility, and high gas permeability, sensors comprising carbon and nanomaterials, which have high sensitivity and mechanical properties, were proposed as sensing materials that could be incorporated in these high gas-permeable substrates. However, the selectivity of the sensing target^[18] and low processability that requires surface modification^[19] are issues that must be addressed when considering the expansion of sensor functions. In the future, multimodal sensors with higher selectivity for a larger number of targets and with easy processing will be required.

Ionic liquids (ILs) are promising sensing materials with high selectivity and ease of modification. ILs, also known as room-temperature molten salts, are liquids composed only of anions and cations. They have been applied in the fields of materials science and electrochemistry owing to their electrochemical stability, nonvolatility, flame retardance, and high ionic conductivity.^[20,21] ILs, as one of the sensing materials, have been reported to demonstrate the characteristics of designer solvents that exhibit varying performances by modifying the combination of anions and cations,^[22–24] as well as high sensitivity.^[25] Because of these features, ILs have been applied in humidity,^[26] gas,^[25] and optical^[27] sensors. Polymer electrolytes combining ILs and polymers, called ion gels, have the potential to be a new sensing material that not only has transparency, ultra-flexibility, and high gas permeability, but can also provide high selectivity. Further, the electrical properties of ILs change according to the temperature and humidity. Therefore, the effects of these factors must be considered when using ion gels as sensing materials. Previous studies have developed ion gels that respond to temperature or humidity.^[26,28,29] However, both temperature and humidity affect ion gels, and the existing ion gel sensors cannot isolate these effects. Selective detection of temperature and humidity using ion gel sensors is a fundamental technology for constructing multifunctional ion gel sensors.

Here, we propose a transparent and highly breathable thin-film sensor comprising polydimethylsiloxane (PDMS) thin film, CNT electrodes, and ion gels, which can be applied to various locations, including living bodies, and can selectively detect multiple parameters with high sensitivity. The use of PDMS and ion gel polymers, which are materials with a high gas permeability, enables sufficient permeation of the water that evaporates from the human skin. At the same time, the thin-film structure ensures high visible light transmittance and reduces discomfort when applied. These sensors were fabricated using a simple spray coating method. In this study, as a proof of concept, selective high-sensitivity detection of temperature and humidity was achieved. Our demonstration suggests the possibility of multifunctional sensors that can satisfy the requirements of transparency, ultra-flexibility, and high gas permeability by changing the ILs and the polymers that constitute ion gels.

2. Results and Discussion

A transparent thin-film temperature and humidity sensor that can be attached to various locations, including biological

surfaces, was developed (**Figure 1a**). The sensor consists of two sets of CNT transparent electrodes on a flexible PDMS thin-film substrate. Thickness of the PDMS substrate was $\approx 25 \mu\text{m}$. Hydrophobic and hydrophilic ion gels are deposited on a CNT electrode to form temperature- and humidity-sensitive layers. Ion gels have a structure in which the ILs are compatibilized with the soft segments of the copolymer, and they exhibit the properties of a solid electrolyte that combines the mechanical stability and flexibility of a polymer with the high ionic conductivity of ILs. Hydrophobic ion gels are a combination of trihexyltetradecylphosphonium bis(trifluoromethanesulfonyl) amide ([P66614] [TFSA]), which is an IL with almost no water absorption ability, and poly(vinylidene fluoride-co-hexafluoropropylene) (PVDF-HFP), a polymer with high hydrophobicity. These polymers are electrically stable against humidity owing to their hydrophobic properties. Conversely, hydrophilic ion gels, which respond sensitively to temperature and humidity changes in the air, are a combination of a highly water-absorbent solvate IL (SIL), an equimolar mixture of tetraglyme and lithium bis-(trifluoromethanesulfonyl)amide ([Li(G4)] [TFSA]), and a polyether-polyamide thermoplastic elastomer, Pebax MH 1657. Impedance changes were measured for the following two types of ion gels: hydrophobic ion gel, which responds to temperature changes, and hydrophilic ion gel, which responds to temperature and humidity changes. Further, the data from these ion gels were integrated to enable independent detection of temperature and humidity. Owing to the flexibility of the PDMS thin film, this sensor can be applied at various locations, including the surface of the human body. Moreover, PDMS and ion gels transmit visible light well; consequently, the appearance of the applied area is unaltered (**Figure 1b–d**). Further, the thin-film structure and nanostructure of the polymer allows for the permeation of water vapor that evaporates from the skin owing to the high gas permeability, thus making it suitable for application on living bodies.

The processing method of the sensor is shown in **Figure 1e**. Polyvinyl alcohol (PVA) is used as a sacrificial layer that protects the soft sensing materials from stretching forces during detachment from the substrate. Transparent CNT electrodes and ion gels are deposited by spray coating. Spraying while heating the PDMS substrate is important for the formation of uniform electrodes and ion gels. The developed temperature and humidity sensors are removed from the acrylic substrate using a frame of adhesive tape to maintain their shapes because of extreme flexibility of the sensors.^[30] Finally, the sacrificial PVA layer is dissolved from the removed sensor.

The microstructure and characteristics of the sensor were also investigated. A schematic diagram of the fabricated hydrophobic ion gel sensor is shown in **Figure 2a(i)**. A scanning electron microscope (SEM) image of the CNT electrode is shown in **Figure 2a(ii)**. CNTs were observed to form a random network on the PDMS substrate. The boundary between the CNT electrode and the hydrophobic ion gel was observed via an energy-dispersive X-ray spectroscopy (EDX), and the image is shown in **Figure 2a(iii)**. Fluorine and carbon in PVDF-HFP, which form the ion gel, are concentrated in the ion gel region on the left side of the image. A small amount of carbon from the CNTs and silicon and oxygen from PDMS are distributed in the CNT-PDMS substrate region on the right side of the image.

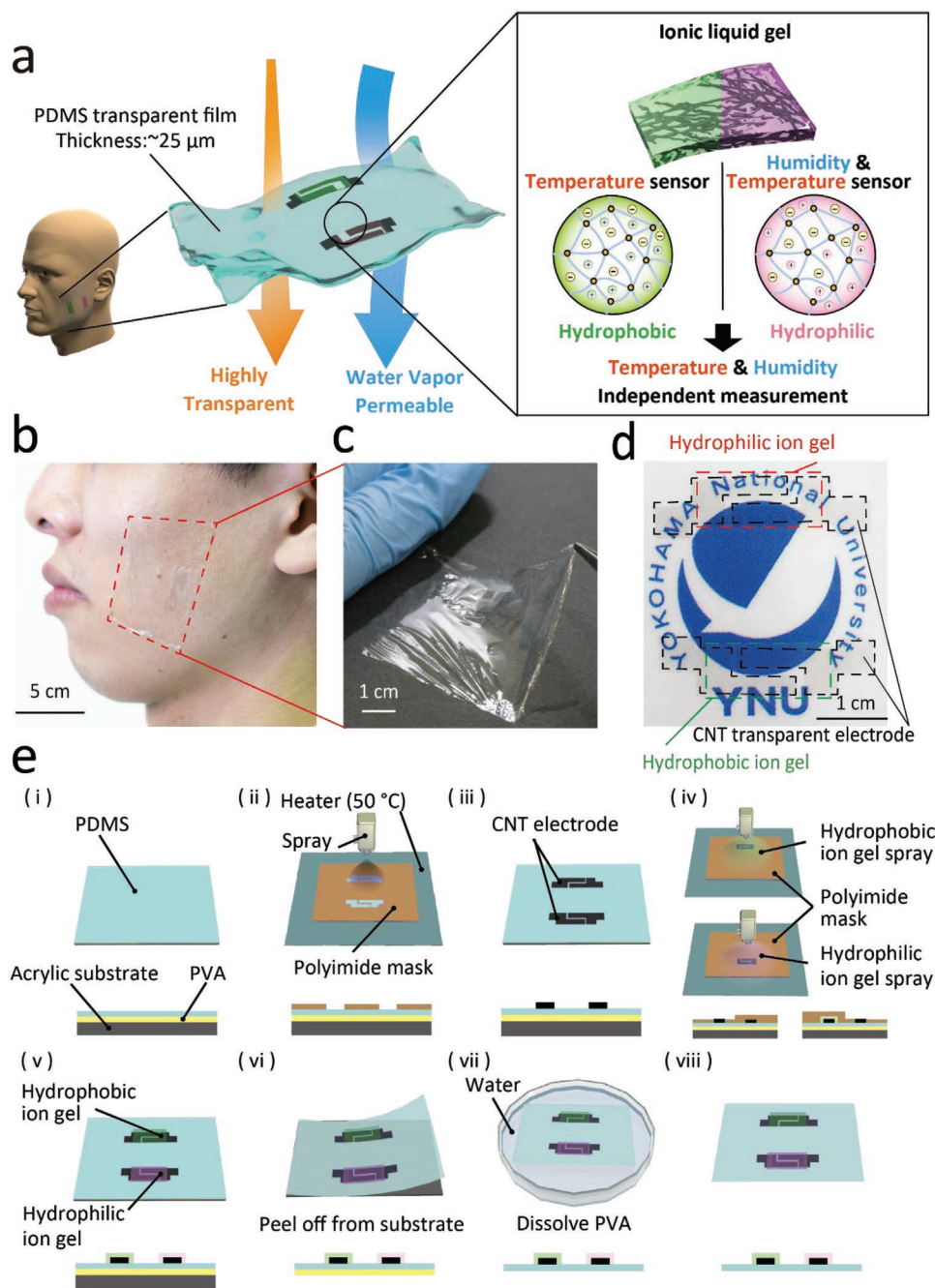


Figure 1. Ion gel-based temperature and humidity sensor that is highly breathable, transparent, and ultra-flexible. a) Concept of the ion gel thin-film temperature and humidity sensors. Temperature is measured by the hydrophobic ion gels. Humidity is measured by the hydrophilic ion gels. Temperature data measured by the hydrophobic ion gel are used to calibrate the impedance change of the hydrophilic ion gel to achieve independent detection of temperature and humidity. b) The ion gel thin-film sensor is attached to the cheek of a male subject. The red dotted line outlines the ion gel thin-film sensor. c) The ion gel thin-film sensor is lifted by tweezers. d) The ion gel thin-film sensor stretched over the printed university logo; polydimethylsiloxane (PDMS) substrate, carbon nanotube (CNT) electrode, and ion gel exhibit high light transmittance. e) The fabrication process of the ion gel temperature and humidity sensors.

The light transmission characteristics of the sensors were also investigated (Figure 2b). In this study, the amount of ion gel deposited by the spray was evaluated in terms of mass per unit area by the thermogravimetric analyzer. It was determined that increasing the number of CNT sprays decreases the light transmittance because of the increased density of CNTs

on the PDMS substrate (Figure S1, Supporting Information), while increasing the number of contacts in the network causes an increase in electronic conductivity (Figure S2, Supporting Information). The raw PDMS substrate showed almost 100% light transmission in visible light (380–780 nm); the composite of CNT electrodes and hydrophilic ion gels deposited

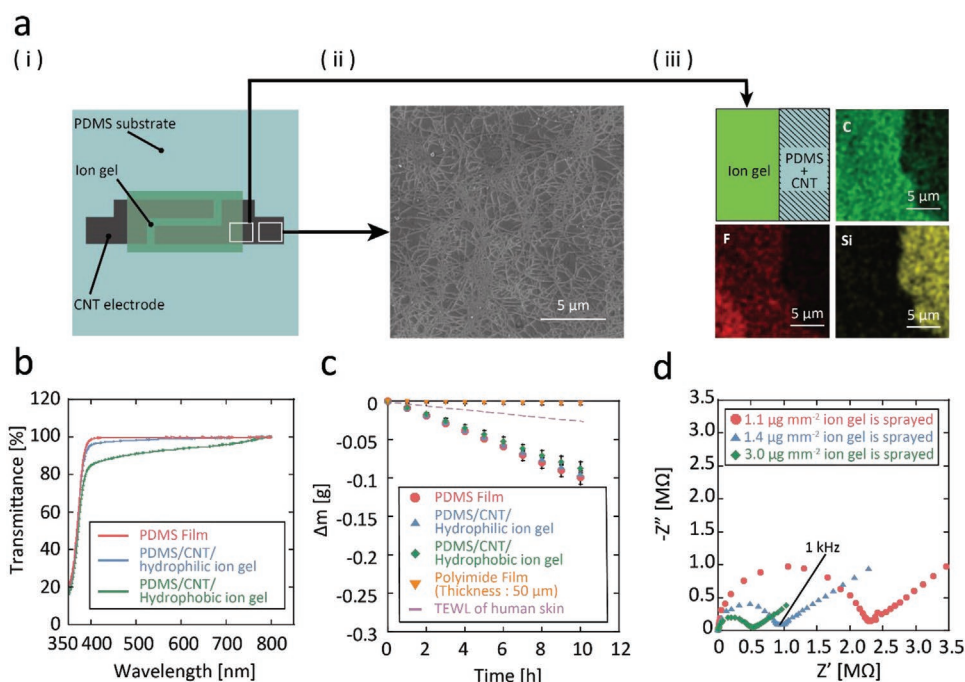


Figure 2. Evaluation of the structure and permeability of the developed thin-film temperature and humidity sensors. a) Scanning electron microscopy (SEM)/energy-dispersive X-ray spectroscopy (EDX) analysis of the ion gel temperature sensor. i) Top view of a schematic of the fabricated ion gel temperature sensor. The white square on the right demarcates the area photographed via SEM-EDX. ii) SEM image of the transparent CNT electrode showing the CNT networks. iii) EDX image of the boundary between the hydrophobic ion gel and the electrode. Polymer-derived fluorine and carbon are observed in the ion gel, and CNT-derived carbon and PDMS-derived silicon are observed in the electrode. b) Light transmission spectrum of the material comprising the thin-film sensor, which transmits >80% of visible light. c) Mass change of a vial containing water sealed by the thin-film sensor; $n = 8$ for PDMS/CNT/hydrophilic ion gel, $n = 9$ for the other samples. The mass loss increases with respect to the gas permeability. The data is shown by mean \pm standard deviation of $n = 8$ or 9. d) Nyquist plot of the hydrophobic ion gel. The final hydrophobic ion gel was measured at 1 kHz as shown in the figure.

in a structure similar to that of the developed sensor showed >90% optical transmission over the entire visible light range, while the composite of PDMS and CNT electrodes with hydrophobic ion gels showed >80% optical transmission over the entire visible light range. The low visible light transmittance of hydrophobic ion gels as compared with that of hydrophilic ion gels is due to the light scattering from relatively large crystallites (spherulites) of the PVDF-HFP network used in the ion gel.^[30,31] Conversely, hydrophilic ion gels prepared using Pebax MH 1657 were reported to have relatively uniform morphology with smaller aggregates of the insoluble polyamide domains;^[32] this contributes less to light scattering. Thus, the use of elastomers with smaller phase-separated domain structures may afford high light transmittance, even in hydrophobic ion gels. In this study, the light transmittance decreased with an increase in the amount of ion gel coating. The light transmittance of hydrophobic ion gels was more affected by the increase in the amount of coating than that of the hydrophilic ion gels (Figure S3, Supporting Information).

The results of the evaluation of the moisture permeability of the developed sensor are shown in Figure 2c. The amount of water vapor that evaporated from a sealed container through each film was measured by observing the mass loss of the entire container (Figure S4, Supporting Information). The developed sensor showed a high-water transmission rate owing to its thin-film-based physical structure and amorphous

chemical structure. Considering the area of the membrane ($1.67 \times 10^{-3} \text{ m}^2$), the water permeation through a unit area per unit time of the hydrophilic and hydrophobic ion gel sensors was 56.9 ± 1.3 and $52.4 \pm 5.1 \text{ g m}^{-2} \text{ h}^{-1}$, respectively (Figure S5, S6, Supporting Information). Transepidermal water loss (TEWL) in the human body is $\approx 15 \text{ g m}^{-2} \text{ h}^{-1}$ on the forearm^[33] and $11 \text{ g m}^{-2} \text{ h}^{-1}$ on the forehead;^[34] therefore, the developed hydrophilic ion gel sensor showed a maximum water transmission rate that was 3.9 times greater than the evaporation rate from the skin. Although the water transmission of hydrophobic ion gels is lower than that of hydrophilic ones, it is still 3.5 times higher than the TEWL of the skin. Furthermore, because the gel occupies only a small percentage of the sensor area, which is predominantly occupied by a PDMS thin film with higher water permeability, the water permeability of the sensor is sufficiently high when compared to the TEWL of the human skin. When the amount of ion gel applied was increased, the water permeability decreased owing to an increase in the film thickness. This is especially noticeable for hydrophobic ion gels. This is caused by the low water permeability of the polymer due to its high crystallinity;^[35] moreover, there is a possibility that the water permeability can be improved by using a polymer with lower crystallinity for the ion gels.

The electrical properties of the hydrophobic ion gels were evaluated using electrochemical impedance spectroscopy in the 7 MHz–1 Hz frequency range and expressed in terms of

complex impedance plots (Nyquist plots) (Figure 2d). A similar Nyquist plot was observed for the hydrophilic ion gel measurements (Figure S7, Supporting Information). The real axis of the semicircular arc in the Nyquist plot is attributed to the ionic conduction resistance of each ion gel (R_{gel}). The assumed equivalent circuit is shown in Figure S8, Supporting Information. In this study, measurements of R_{gel} of the ion gels were performed using a constant frequency alternating current (1 kHz for hydrophobic ion gels and 400 Hz for hydrophilic ion gels), where the imaginary impedance was close to zero at the measured temperature and humidity.

R_{gel} obtained in the experiment (Figure 2d) decreases with an increase in the amount of the ion gel sprayed. The decrease in R_{gel} can be explained by the increase in the ionic conduction path. The ion gels deposited by spray coating, as in this study, do not form films of uniform thickness, unlike the defect-free bulk films prepared by spin coating or other methods. In the case of spray coating, several sprayed gel droplets bond with each other to form a network and generate conduction paths. As the spray volume increases, the network becomes denser, and the increase in the ionic conduction path is caused by an increase in the ion gel thickness and the formation of net-

works between the ion gel droplets. Therefore, R_{gel} of the ion gel changes nonlinearly with the spray volume. In accordance with the purpose of this study, we decided to use a membrane fabricated by spraying the hydrophilic ion gel for 6 s (mass: $0.80 \mu\text{g mm}^{-2}$) as a humidity sensor, considering the spray time of the hydrophilic ion gel, light, and water vapor permeability, linearity, and sensor sensitivity listed in Table S1, Supporting Information. In addition, considering the spray time of the hydrophobic ion gel provided in Table S2, Supporting Information, together with the light and water vapor permeability, and stability against humidity, it was decided to fabricate the membrane by spraying the hydrophobic ion gel for 10 s (mass: $1.4 \mu\text{g mm}^{-2}$) as the temperature sensor. The coating method used in this experiment is optimized for the purpose of this study. Therefore, it is necessary to alter the method depending on the intended use and device requirements.

The properties of the hydrophobic ion gel as a temperature sensor were evaluated (Figure 3a). The operating principle of the hydrophobic ion gel temperature sensor is illustrated in Figure S9, Supporting Information. Hydrophobic ion gels have low water absorption, and the impedance variation due to humidity changes is small. In contrast, the ion mobility, which

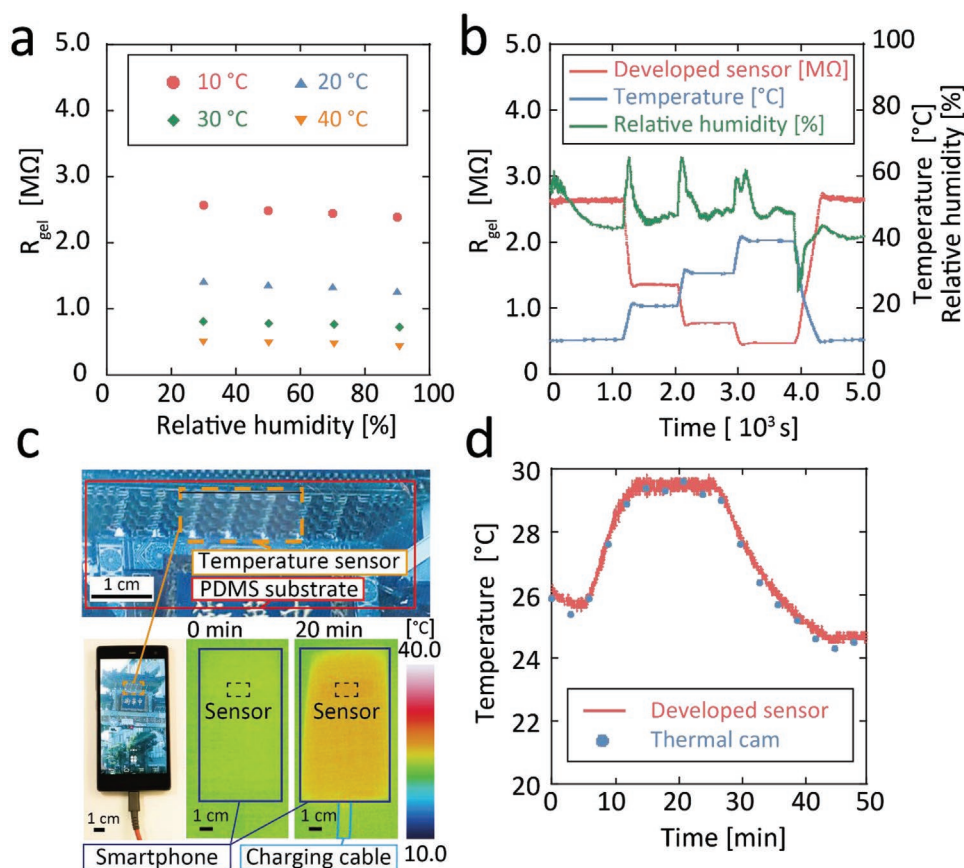


Figure 3. Thin-film temperature sensor using the hydrophobic ion gel. a) R_{gel} of the ion gel temperature sensor changes when the humidity is varied at a constant temperature. b) Impedance of the ion gel temperature sensor changes when the temperature in the environmental chamber is continuously changed from 10 to 40 °C (left axis); the temperature and humidity were recorded by a commercial sensor (right axis). The developed temperature sensor is unaffected by changes in the humidity and responds well to changes in the temperature. c) Photograph and thermal image of a smartphone with the ion gel temperature sensor attached to the screen. Owing to its high light transmittance, the sensor does not obscure the image on the liquid crystal display. d) Changes in temperature are measured by attaching the sensor to the smartphone screen over time. The results correspond well with the temperature changes measured by the thermal camera.

controls the conductivity of hydrophobic ion gels, increases with increasing temperature owing to the activation of molecular motion.^[36] Thus, a sensor that is less sensitive to humidity and more sensitive to temperature changes can be fabricated. In the temperature range of 10–40 °C, the R_{gel} of the developed temperature sensor was affected by $\pm 4.8\%$ when the humidity varied in the range of 30%–90%. The temperature around the ion gel sensor continuously varied from 10 to 40 °C, and the results were compared with those of commercial sensors (Figure 3b). The sensor showed a nonlinear response to temperature. The sensitivity of the temperature sensor, calculated by an existing method,^[37] was $15.4\% \text{ } ^\circ\text{C}^{-1}$ at 25 °C. The sensor

exhibited lower sensitivity to humidity, stable output, and good resilience in response to changes in temperature.

For a demonstration of the hydrophobic ion gel temperature sensor, we attached the sensor to the screen of a smartphone and measured the temperature change during battery charging (Figure 3c). The attachment of the sensor to the liquid crystal display did not block the view of the screen, and the displayed image could be viewed through the sensor. The temperature increase in the smartphone was observed using a thermal camera and compared with the displayed temperature of the sensor (Figure 3c,d). The output signal of our temperature sensor corresponded well with the observed results of

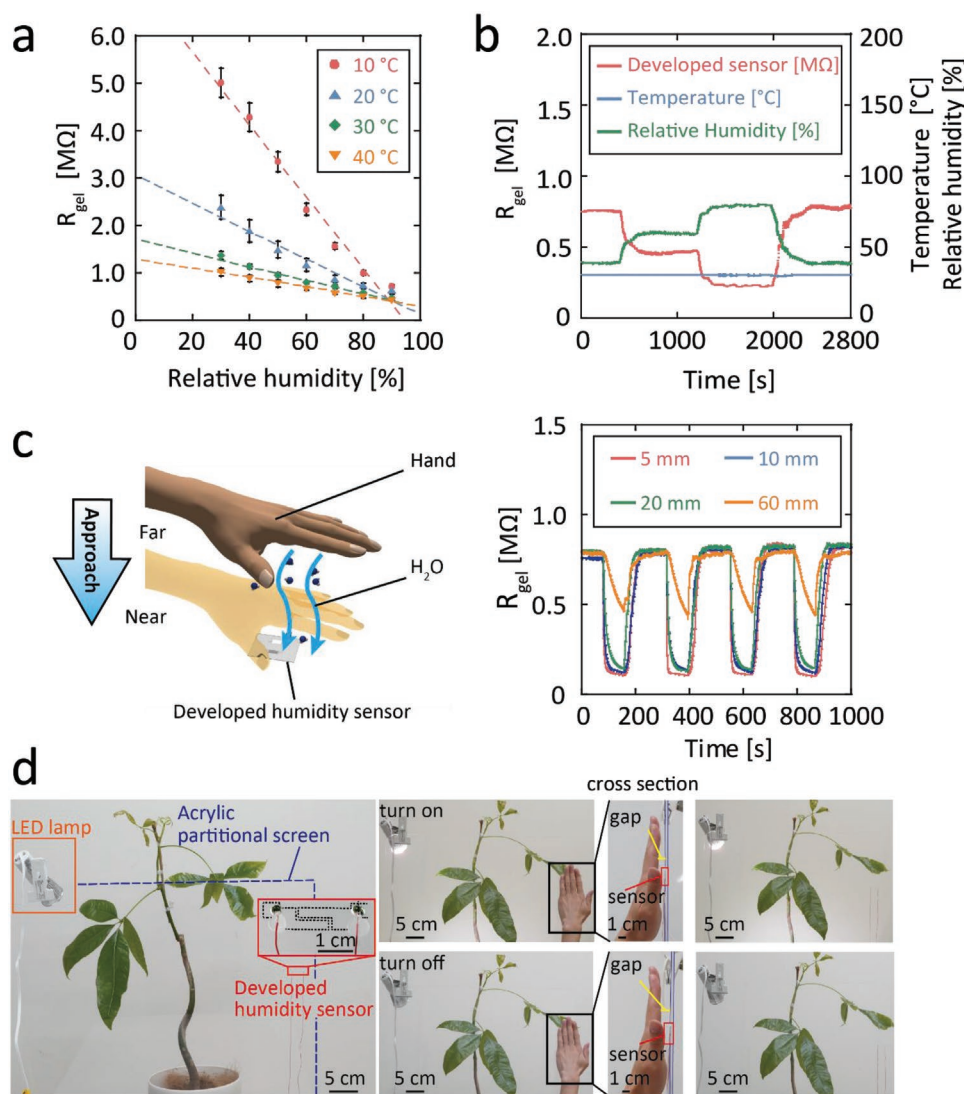


Figure 4. Thin-film humidity sensor using the hydrophilic ion gel. The impedance of the sensor demonstrates a decreasing tendency with respect to temperature. a) Changes in R_{gel} of the ion gel against the humidity at 10, 20, 30, and 40 °C. The data is shown as mean \pm standard deviation of $n = 300$. The variation in impedance due to changes in the humidity decreases as the temperature increases. b) R_{gel} of the ion gel humidity sensor (left axis) when the humidity in the environment chamber is continuously varied from 40% to 80% at a constant temperature of 30 °C; temperature and humidity changes are recorded using a commercial sensor (represented by the axis on the right). c) Schematic of proximity sensing by the ion gel thin-film humidity sensor and impedance changes in the ion gel humidity sensor for different distances between the hand and the sensor when the hand changes position by moving back and forth. d) Demonstration of proximity switching using the ion gel thin-film humidity sensor. Noncontact switching of light-emitting diode (LED) lights triggered by the increase in the ambient moisture content due to the proximity of a hand.

the thermal camera, and an increase in the temperature of the smartphone due to battery charging was observed.

The integration of a transparent temperature sensor with a smartphone can be used not only to detect thermal runaway but also to prevent fingerprint copying^[9] in on-screen fingerprint authentication processes.

The characteristics of the hydrophilic ion gel as a humidity sensor were evaluated (Figure 4a). The sensitivity of the sensor was calculated using Equation (1).

$$S = \frac{Z_{30\%} - Z_{90\%}}{Z_{50\%}} \times 100 \times \frac{1}{90 - 30} \quad (1)$$

where S is the sensitivity, $Z_{30\%}$, $Z_{50\%}$, and $Z_{90\%}$ are the impedances at each relative humidity (RH) level.^[29] The rate S at which the impedance of the ion gel humidity sensor changed was calculated as 2.0% per RH% at 20 °C using Equation (1). The coefficients of determination in the linear approximation are $R^2 = 0.9783$, 0.9482, 0.9760, and 0.9869 at 10, 20, 30, and 40 °C, respectively, with high linearity (Figure 4a). This is because of the ionic-conduction-based humidity measurement principle of the developed sensor (Figure S10, Supporting Information). Resistive humidity sensors of the polymer and ceramic types measure the conductivity caused by proton hopping in the layer of adsorbed water molecules.^[38] Therefore, in the low humidity range where insufficient water molecules are adsorbed, the high bulk resistance inherent to ceramics and polymers is output. The change in resistance between the high and low humidity ranges can reach over 100 times, resulting in low linearity. Conversely, in the proposed humidity sensor, the ionic conductivity of the SIL supported by the polymer dominates the output value in all humidity ranges. The phenomenon of ILs adsorbing water molecules and significantly decreasing their viscosity was previously reported, which is speculated to be due to the decrease in electrostatic interactions between ions associated with water adsorption.^[39] The same phenomenon was thought to occur in the developed sensor. The hydrophilic SIL [Li(G4)] [TFSA] adsorb water molecules and their viscosity decreases, which increases ionic conductivity and consequently decreases R_{gel} . Because the SIL in the polymer is responsible for conduction even in the low humidity range, a sudden increase in impedance in the low humidity range, which is generally observed in polymer-only- or ceramic humidity sensors, does not occur, resulting in high linearity (Figure 4a). The linearity of the sensor output is an important parameter because it reduces the complexity of the processing system when analyzing the measurement data.

The sensor was compared with a commercial sensor by maintaining the ambient temperature at 30 °C and continuously varying the RH around the ion gel humidity sensor to 40%, 60%, and 80% (Figure 4b). The results of the ion gel humidity sensor corresponded well with that of the commercial sensor and showed good recovery performance.

To demonstrate the fast response of the ion gel humidity sensor, a noncontact switching demonstration was conducted (Figure 4c,d). When a hand approaches the ion gel humidity sensor, the impedance of the sensor decreases rapidly as the ion gel humidity sensor absorbs the moisture dissipated from the hand as mentioned in the citation.^[10,29] (Figure 4c).

We evaluated the response of the ion gel humidity sensor depending on the distance between the hand and the sensor. The response time was defined as the time from the approach of the hand until the impedance reached 90% of the minimum value. The recovery time was defined as the time from the removal of the hand until the impedance reached 10% of the minimum value. When the distance between the hand and the sensor was 5 mm, the average response and recovery times for the four experiments shown in Figure 4c were 6.8 and 49.1 s, respectively. The same experiment was conducted by changing the distance to 10, 20, and 60 mm. As the distance between the hand and the sensor increased, the time required for water molecules to diffuse and reach the sensor increased, resulting in a delay in the time required to reach saturation.

To compare the performance of the ion gel humidity sensor with that of the ion gel temperature sensor, the same experiment was conducted using an ion gel temperature sensor (Figure S11a, Supporting Information). The reaction and recovery times of the ion gel temperature sensor were observed to be 57.9 and 33.9 s, respectively. From these results, we can conclude that the fast response time of the ion gel humidity sensor is due to the adsorption of water molecules and not due to temperature change.

A CNT thin-film humidity sensor was fabricated using the same CNTs used for the electrode as the humidity sensing part, excluding the hydrophilic ion gel. A proximity sensing experiment, similar to that of the ion gel humidity sensor, was conducted to compare its performance with that of the ion gel humidity sensor (Figure S11b, Supporting Information). The reaction and recovery times of the CNT thin-film humidity sensor were 50.4 and 78.1 s, respectively. The impedance change from the initial value to the maximum value of the ion gel humidity sensor was -86%, while that of the CNT-only humidity sensor was +6.6%. In comparison with the CNT-only humidity sensor, the ion gel humidity sensor using [Li(G4)] [TFSA] is superior in terms of sensitivity and reaction speed.

As a proof of concept, an LED light was controlled by noncontact switching using an ion gel humidity sensor (Figure 4d). An enlarged cross-sectional view of the distance between the hand and the sensor is shown in Figure S12, Supporting Information. The ion gel humidity sensor was attached to a transparent acrylic partitioning screen, and the LED light was successfully switched on and off by a program based on the impedance reduction caused by the approach of the hand (Figures S13 and S14, Supporting Information). The ion gel thin-film humidity sensor is a transparent and flexible thin-film sensor that can be affixed to various places, such as windows, partitioning screens, and the human body, without any change in appearance and can be switched on and off without contact. Therefore, noncontact switching using an ion gel transparent thin-film humidity sensor is expected to be applied to smart windows and noncontact input interfaces, such as transparent buttons and keyboards.

By integrating the developed temperature and humidity sensors on the same plane, we evaluated the selective detection of temperature and humidity (Figure 5). The impedance of the ion gel humidity sensor changes due to two factors: the change in viscosity caused by the adsorption of water molecules^[39] and the change in ion mobility caused by the change

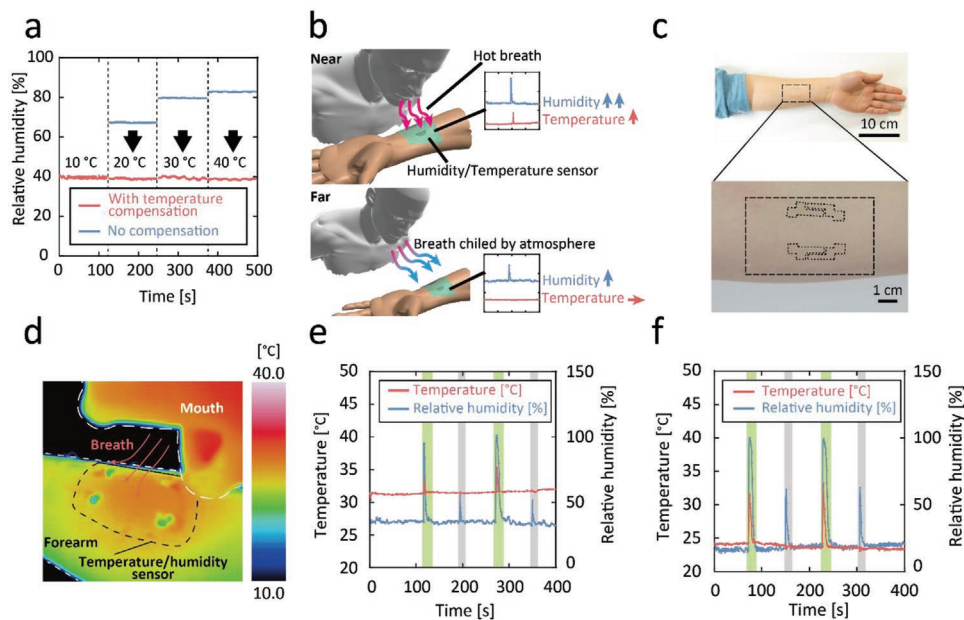


Figure 5. Demonstration of independent detection of temperature and humidity using the ion gel thin-film sensor. a) Comparison of the output values of the ion gel humidity sensor with and without temperature compensation at 40% relative humidity (RH). Accurate output can be obtained by using the ion gel temperature sensor for temperature compensation. b) Schematic diagram demonstrating the detection of the temperature of breath. The ion gel temperature and humidity sensors attached to the forearm detect the temperature and moisture content of exhaled air. Both the temperature and humidity sensors respond to air exhaled at short distances; however, the temperature sensor does not respond to air exhaled at long distances because it is cooled; therefore, only the humidity sensor shows a response. c) Ion gel thin-film temperature and humidity sensors applied to the forearm. The flexibility of the sensor allows it to be attached to a forearm with a curvature. d) Thermal camera image of breath exhaled at a short distance in a refrigerated room. The overall skin temperature decreases; however, it increases only in the area affected by the exhalation. The low-temperature point on the sensor is the contact part connecting the wires and sensor. Results of exhalation detection experiment at e) room temperature, and f) in the refrigerated room. The green area shows exhalation from a short distance, and the gray area shows exhalation from a long distance.

in temperature.^[25] This causes a change in the characteristics of the humidity sensor depending on the ambient temperature, as shown in Figure 4a. When the measurements do not take into account the crosstalk between temperature and humidity, the RH value differs significantly from the accumulated value (Figure 5a, solid blue line). Therefore, accurate humidity values can be obtained from the calibration curve of humidity in the ion gel humidity sensor with respect to the temperature after the temperature is determined using the temperature sensor (Figure 5a, solid red line, Figure S15, Supporting Information). As a proof of concept for a transparent thin-film sensor that independently detects temperature and humidity, the respiratory temperature was measured by attaching sensors to the forearm of a human body (Figure 5b,c). The body surface temperature at room temperature is ≈ 32 °C, and the temperature of the exhaled air is ≈ 34 °C. Therefore, when breathing very close to the sensor, the temperature, and humidity increase because of the moisture contained in the exhaled air, causing both the ion gel temperature and humidity sensors to respond. Conversely, when breathing away from the sensor, the exhaled air is cooled by the surrounding air; consequently, the temperature sensor does not respond, but the moisture content increases, and only the humidity sensor responds. Independent detection of temperature and humidity can be demonstrated by discriminating between these two types of breathing. To prove that the sensor can respond to changes in the skin temperature caused by outside temperature, measurements

were conducted at room temperature (25 °C, 50 RH%) and in a refrigerated room (4 °C, 80 RH%). In the refrigerated room, the skin temperature decreased to 24 °C, and the increase in skin temperature due to exhalation was clearly confirmed using a thermal camera (Figure 5d). The results of the measurements at room temperature (Figure 5e) and in the refrigerated room (Figure 5f) were compared. At room temperature, the skin temperature was ≈ 32 °C without the influence of respiration; however, it decreased to 24 °C in the refrigerated room. A thin-film temperature sensor could also observe a gradual decrease in skin temperature caused by a long stay in a low-temperature environment. The temperature sensor that received exhaled air from a short distance exhibited an increase in temperature at both room and cold temperatures. At room temperature, the maximum values when breathing from short and long distances were 33 and 35 °C, respectively. In the low-temperature environment, the maximum values were 31 and 33 °C, respectively. The lower maximum temperature in the low-temperature environment can be explained by the fact that the ambient environment cools the exhaled air even at short distances. The humidity detected by the sensor that received exhaled air from a short distance increased to almost 100% in both room- and low-temperature environments. Because the humidity of the air exhaled by humans is considered to be almost 100%, it can be said that water molecules did not diffuse into the atmosphere and reached the sensor because of the close distance.

The temperature sensor that received the exhaled air from a long distance did not change its output value at either room or cold temperatures. Because the air exhaled from a distance was cooled by the atmosphere and the temperature reduced to a value equivalent to that of the ambient environment by the time it reached the sensor, the skin temperature, which was higher than that of the ambient environment, dominated the output value of the ion gel temperature sensor, and no temperature change occurred. Conversely, the humidity sensor that received the air exhaled from a long distance showed an increase in humidity at both room and cold temperatures. Because some of the water molecules contained in the exhaled air diffused into the air before reaching the sensor, a smaller change in humidity was observed than the case where the air was exhaled from a short distance. Two experiments were each conducted at room and low temperatures; the maximum humidity values of the ion gel humidity sensor when the air was exhaled from long distances at room temperature were 52% and 56%, respectively, whereas the maximum humidity at low temperature was 62% and 63%, respectively. This is because the saturated water vapor content is smaller in the low-temperature environment; therefore, the humidity change is larger even with the same increase in water vapor content. These comparisons prove that the ion gel transparent temperature sensor operates independently in detecting humidity, and temperature- and humidity-independent detection is possible by correcting the ion gel humidity sensor that responds to temperature and humidity. The technology for independent detection of temperature and humidity on human skin may be used in the future to detect perspiration and fever, and for alerts against heatstroke.

When compared to other studies based on ion conductors and carbon materials, the thin-film temperature sensor developed in this study has high sensitivity. Moreover, the temperature sensor possesses both high gas permeability and stability against humidity. To fabricate a temperature sensor that is stable against humidity changes, it is necessary to use a material that is not affected by moisture, such as metal,^[40] or to coat the sensor to protect it from moisture intrusion.^[41] As metallic materials are not gas permeable and protection against moisture penetration directly blocks gas permeation, it was difficult to fabricate a breathable temperature sensor. In this study, we achieved both air permeability and independence from humidity in the sensor by using the hydrophobic properties of the thermosensitive material.

A comparison between similar studies and our study is presented in Table S3, Supporting Information. The humidity sensor developed in this study exhibits linear sensitivity and also has both high light permeability and flexibility. It should be noted that this is the first transparent and flexible humidity sensor that considers gas permeability. Previous gas-permeable humidity sensors^[13] did not have transparency, and this research surpasses them in terms of sensitivity. Among the sensors developed in extant studies, humidity sensors using cellulose + KOH^[10] could exhibit gas permeability. It is also independent of temperature changes and exhibits transparency, which is highly similar to the concept used in this study. However, our sensor has an advantage in terms of its high linearity and the ability to be directly attached to a living body because of the biocompatibility of the PDMS substrate. A previously

developed graphene oxide/graphene/PDMS-based sensor^[41] was a transparent thin-film sensor with independent detection of temperature and humidity, and because of the use of the PDMS substrate, this sensor could have gas permeability. However, our sensor has an advantage in terms of reaction speed, as well as high processability, which does not require a PDMS covering to protect the temperature sensor from humidity interference. Therefore, our ultra-flexible thin-film sensor using ion gel surpasses the all-carbon sensors in terms of high selectivity and good processability.

It might not be appropriate to create a sensor using ion conductors that measures temperature independent of humidity because the conductors possess a high affinity to water. However, the fact that two types of transparent thin-film sensors with different functions (temperature and humidity) were achieved by changing the combination of ILs and polymers in this study is of great significance. This suggests the high expandability of our method, which can be used to fabricate more diverse types of ion gel thin-film sensors. Various ILs that have already been applied as gas sensors^[25] and optical sensors^[27] have been reported. Various developments of these sensors might be possible, such as improving the reaction speed by implementing ILs into thin-film sensors using our methods. Furthermore, temperature and humidity sensors are fundamental technologies for the expansion of IL sensors because sensors using ILs are strongly affected by the temperature and humidity of the environment. Thus, this study introduces the possibility of fabricating temperature and humidity sensors for compensation and an extended IL sensor with a simple and consistent processing method.

3. Conclusion

In summary, a transparent, gas-permeable, flexible, ion gel thin-film temperature and humidity sensor was developed using a simple spray coating method. The sensors have a high optical transmittance of >80% in the visible light range because of their thin physical structure and the chemical structure of ion gels, moisture transmittance of the sensors is 3.5 times higher than the TEWL of the human body. The ion gel temperature sensor, which is based on the activation of ionic motion associated with the temperature change, showed a stability of $\pm 4.8\%$ in response to humidity change. By using hydrophobic materials, it was possible to fabricate a temperature sensor with high selectivity to humidity without using a water vapor protective film for protection. The ion gel humidity sensor, which is based on the viscosity change of the IL due to the adsorption of water molecules, showed an impedance change of 2.0% per RH%, which is a good sensitivity for a sensor with high linearity. Although the output of the ion gel humidity sensor depends on temperature, selective detection of temperature, and humidity by the ion gel thin-film sensor was achieved by compensating values from the humidity sensor based on the temperature sensor. Our results show that gas-permeable transparent flexible sensors can be easily fabricated using ion gels; moreover, selective sensing of multiple targets is possible by the appropriate selection of ion gel materials. In the future, it is expected that chemical sensing will be performed using ion gels

with various types of ILs. In addition, the easy processability of full-printing processes is expected to enable the mass production of multifunctional sensors via printing in the future.

4. Experimental Section

Preparation of PDMS Thin-Film Substrates: PDMS thin-film substrates were prepared by spin-coating. First, PVA (Kanto Chemical) was mixed with deionized water (100 mL) and stirred at 200 °C for 1 h to dissolve it and obtain a 10 wt% PVA solution. The PVA solution was spin-coated on an acrylic substrate at 1000 rpm for 40 s using a spin coater (MS-B100, MIKASA), and then dried in an oven at 70 °C for 1 h to prepare the sacrificial layer. The PDMS solution was prepared by mixing PDMS (1 g; KE-1606, Shin-Etsu Chemical Company), hexane (2.4 g; Fujifilm Wako Chemical Co., Ltd.), and ethyl acetate (0.6 g; Fujifilm Wako Chemical Co., Ltd.). The solution was first mixed in a self-rotating mixer (ARE-310, Thinky) for 2 min and then stirred at room temperature for 30 min to produce a uniform PDMS solution. PDMS substrates were fabricated by spin-coating the PDMS solution onto the PVA sacrificial layer at 2000 rpm for 40 s, followed by drying in an oven at 70 °C for 2 h.

Fabrication of CNT Transparent Electrode: The CNT transparent electrodes were fabricated on a PDMS substrate using the spray coating method. First, a polyimide film (3M, 50 μm thickness) was cut using a laser marker (MD-T1000W, Keyence) to create a stencil mask of the electrode pattern. The mask was placed on the PDMS substrate and treated with excimer for 60 s using a small excimer equipment (L12530-01, Hamamatsu Photonics). Then, 0.05 wt% CNT dispersion (EC-DL, Meijo Nano Carbon Co., Ltd.) was sprayed on the PDMS substrate using a homemade spray coater (Figure S16, Supporting Information). The spraying process was performed when the substrate was heated to 50 °C; moreover, the spray pressure was 0.3 MPa, the distance between the spray and the substrate was 15 cm, and the movement speed of the stage was 300 mm s⁻¹. After spraying, the CNT transparent electrode pattern was obtained by peeling off the mask.

Fabrication of Ion Gel Transparent Temperature and Humidity Sensors: The ion gel temperature sensor was fabricated on a CNT electrode using the spray coating method. First, PVDF-HFP (Arkema) was diluted to 0.5 wt% in dehydrated acetone (Fujifilm Wako Chemical Co., Ltd.) in a vial and stirred at room temperature for 1 h. Next, [P66614] [TFSA] (Fujifilm Wako Chemical Co., Ltd.) was added dropwise to the polymer solution to make PVDF-HFP: [P66614] [TFSA] = 1:4 (mass ratio), which was further mixed at room temperature for 30 min to prepare the ion gel solution. The ion gel was deposited by spraying the ion gel solution on the electrode using a stencil mask composed of a polyimide film prepared in the same way as the mask for the CNT electrodes. The spraying process was performed while the substrate was heated to 35 °C; the spray pressure was 0.2 MPa, and the distance between the spray and the substrate was 15 cm. The stage was fixed, and spraying was performed with a 5 s interval between every 2 s of spray time. After spraying, the mask was peeled off to obtain a transparent temperature sensor.

The ion gel humidity sensor was prepared in a similar manner as the temperature sensor. SIL [Li(G4)] [TFSA] was synthesized by mixing equimolar amounts of [Li] [TFSA] (Kishida Chemical Co., Ltd.) and tetraglyme (Kishida Chemical Co., Ltd.) in a glove box under argon atmosphere and stirring overnight at room temperature in air. Pebax MH 1657 (Arkema) was mixed in an ethanol/water mixture (7:3 mass ratio) in a vial and stirred at 90 °C for 1 h to obtain a 0.5 wt% polymer solution. Next, [Li(G4)] [TFSA] was added dropwise to the polymer solution at a ratio of Pebax:[Li(G4)] [TFSA] = 1:4 (mass ratio), which was further mixed at room temperature for 30 min to prepare the ion gel solution. A stencil mask made of polyimide film, which was prepared using a process similar to that used when the temperature sensor was fabricated, was used to prevent the mixing of the two types of gels. To improve the deposition of ion gels, the electrodes for the hydrophilic ion gel were treated with an excimer for 60 s. Subsequently, the ion gel was

deposited by spraying an ion gel solution on the electrode. The spraying process was performed while heating the substrate to 45 °C; the spray pressure was 0.2 MPa, and the distance between the spray and the substrate was 15 cm. The stage was fixed, and spraying was performed with a 5 s interval between every 2 s of spray time. After spraying, the mask was peeled off to obtain a transparent humidity sensor. Finally, the fabricated ion gel temperature and humidity sensors were dried in a vacuum at room temperature for 3 h to remove the solvent.

Observation of Surface Properties: The fabricated sensor was observed from the top by field-emission SEM (SU8010, Hitachi) at an acceleration voltage of 1 kV. EDX images were obtained using the SU8010 microscope at an acceleration voltage of 3 kV.

Examination of Visible Light Transmission and Moisture Permeability: The light transmittance of the sensor was measured using an ultraviolet-visible light spectrophotometer (UV-2700, Shimadzu). The water permeability of the sensor was measured from the mass loss due to the evaporation of water through the thin film. PDMS films were prepared by the aforementioned method, PDMS films with CNTs and ion gels were deposited on all surfaces, and polyimide films were used. Three types of films, excluding the polyimide film, were peeled off from the acrylic substrate using a frame of adhesive tape (No.7082#25, TERAOKA SEISAKUSHO Co., Ltd), and the PVA sacrificial layer was removed by bringing only the PVA surface into contact with the water surface. Vials containing deionized water (10 ml) were sealed by affixing each film to the mouth of the vial (Figure S4, Supporting Information). The three types of membranes, excluding the polyimide film, were attached to the vial by the intermolecular forces of the PDMS thin film, and the polyimide film was attached to the rim of the vial using an adhesive. These vials were placed in an environmental chamber (SH-241, ESPEC) that was maintained at 25 °C and 30% RH for 10 h. The mass of each vial was measured hourly.

Evaluation of Sprayed Amount of Ion Gels: The gravimetric evaluation of the sprayed ion gels was performed using a thermogravimetric analyzer (STA7200, Hitachi High-Tech Science Co., Ltd). The ion gels were sprayed onto copper foil for 2, 6, 10, and 20 s and maintained at a maximum temperature of 500 °C for 10 min in the thermogravimetric analyzer, after which the reduced mass was measured.

Evaluation of Electrical Characteristics: The Nyquist plot of the ion gel was measured using an impedance analyzer (SP-300, Biologic). Ion gels were deposited on the CNT electrodes. Frequency sweeps were performed in the range of 7 MHz–1 Hz using an impedance analyzer, and the impedance at each frequency was measured. All characterizations were performed at <1 V to prevent chemical reactions.

The electrical properties of the CNTs were measured using an inductance–capacitance–resistance (LCR) meter (ZM2376, NF Corporation). The resistance was measured by connecting the LCR meter to both ends of the CNT electrode.

Measurement of the Sensing Properties of the Temperature and Humidity Sensors: The transparent temperature and humidity sensors were placed inside the environmental chamber without being peeled off from the acrylic substrate and connected to the LCR meter. The impedance of the temperature sensors was measured at 30%, 50%, 70%, and 90% RH at different temperatures. The impedance of the humidity sensors was measured at 30% to 90% RH at different temperatures. Impedances of the temperature and humidity sensors were measured using alternating currents of 1 kHz and 400 Hz, respectively.

Temperature-Measurement Experiment on a Smartphone: The temperature sensor was peeled off from the acrylic substrate using a frame of adhesive tape, and the sacrificial layer was removed. Then, the dried temperature sensor was attached to the screen of a smartphone (Fujitsu F-01F). The sensor was connected to the LCR meter, and the impedance change of the sensor was measured while the battery of the smartphone was charged. The smartphone was simultaneously photographed using a thermal camera (F50B-STD, NIPPON AVIONICS), and the output was compared with the output value of the thin-film temperature sensor.

Proximity Switching Demonstration: Sil-poxy (Smooth-On Inc.) was used to fix the copper wire, which is the connector to the LCR meter, to

the PDMS substrate of the transparent humidity sensor. The transparent humidity sensor with the fixed copper wire was peeled off from the acrylic substrate, similar to the temperature-measurement experiment on a smartphone. After dissolving the sacrificial layer, the sensor was attached to the acrylic partition and connected to the switching system described below. An overview of the switching system is shown in Figures S13 and S14, Supporting Information. The computer triggered the impedance measurement using the LCR meter, judged whether the switching conditions were satisfied, and sent commands to the Arduino microcontroller, which was programmed to switch the relay on/off whenever it received a command. When the impedance of the sensor decreased for two consecutive cycles due to the proximity of the hand, the computer sent a command to the Arduino microcontroller via the serial communication port to switch the relay on/off. The relay was connected to the power source line of the LED light, and the switching of the relay switched on/off the LED light.

Breath Temperature Measurement Experiment: Temperature and humidity sensors attached to the skin were fabricated using the method described in the fabrication of the transparent temperature and humidity sensors. The sensor was peeled off from the acrylic substrate using a frame of adhesive tape, the sacrificial layer was dissolved and dried, and then the sensor was attached to the forearm of a healthy male, in his twenties, with the sensing surface as the upper surface. The distance between the sensor and the face was set to near (3 cm) and far (30 cm) distance measures, and the exhalation was alternately performed from near and far at regular intervals. The impedance changes in the temperature and humidity sensors were measured using the LCR meter, and the obtained data were integrated to calculate the temperature and humidity independently.

Experiments with Human Research Participants: The research protocol was approved by the ethics committee of the Yokohama National University Graduate School of Engineering Science (no.2020-16, approved on 12 February 2021). This study was carried out in accordance with the Declaration of Helsinki and the Japanese Ethical Guidelines of the Ministry of Health, Labor, and Welfare, Japan. Measurements were performed on adult males. After informed consent from all participants, the developed devices were placed on their forearms and faces. The measurement data were collected by a PC. To protect the privacy of the participants, personally identifiable information was stored securely in the laboratory.

Statistical Analysis: Data on water vapor transmission were obtained for $n = 9$ samples. Data are expressed as mean \pm standard deviation for $n = 8$ or 9 samples (Figure 2c), Figure S5 S6, Supporting Information).

The data for the humidity sensor was obtained by performing the experiment shown in the Measurement of the Sensing Properties of the Temperature and Humidity Sensors section three times for the same sensor. 100 data were obtained for each humidity in each experiment, one second apart, and finally 300 data were obtained for a single temperature/humidity pair. Data were expressed as the mean \pm standard deviation of the 300 data (Figure 4a). Approximate straight lines were created by the method of least squares (Figure 4a). All statistical processing was performed by Microsoft Excel.

Supporting Information

Supporting Information is available from the Wiley Online Library or from the author.

Acknowledgements

This work was supported by the PRESTO/Japanese Science and Technology Agency (JST) (Grant Number JPMJPR18J2), JST CREST (Grant Number JP19209665), JST Fusion Oriented Research for Disruptive Science and Technology (FOREST, JPMJFR203Q), the Japan Society for Promotion of Science (JSPS) KAKENHI grants (20H00213,

18H05469, 21H03815), and the Japan Agency for Medical Research and Development (AMED) (Grant Number 21ak0101148j0001). We would like to thank Editage (www.editage.com) for English language editing.

Conflict of Interest

The authors declare no conflict of interest.

Data Availability Statement

Research data are not shared.

Keywords

carbon nanotubes, ionic liquids, polymer electrolytes, polymer thin films, transparent electronics

Received: February 9, 2022

Revised: April 29, 2022

Published online:

- [1] M. Ramuz, B. C. K. Tee, J. B. H. Tok, Z. Bao, *Adv. Mater.* **2012**, *24*, 3223.
- [2] B. W. An, S. Heo, S. Ji, F. Bien, J. U. Park, *Nat. Commun.* **2018**, *9*, 2458.
- [3] T. Q. Trung, L. T. Duy, S. Ramasundaram, N. E. Lee, *Nano Res.* **2017**, *10*, 2021.
- [4] S. R. Kim, J. H. Kim, J. W. Park, *ACS Appl. Mater. Interfaces* **2017**, *9*, 26407.
- [5] Y. Cao, Y. J. Tan, S. Li, W. W. Lee, H. Guo, Y. Cai, C. Wang, B. C. K. Tee, *Nat. Electron.* **2019**, *2*, 75.
- [6] D. J. Lipomi, M. Vosgueritchian, B. C. K. Tee, S. L. Hellstrom, J. A. Lee, C. H. Fox, Z. Bao, *Nat. Nanotechnol.* **2011**, *6*, 788.
- [7] E. Roh, B. U. Hwang, D. Kim, B. Y. Kim, N. E. Lee, *ACS Nano* **2015**, *9*, 6252.
- [8] P.-C. Chen, S. Sukcharoenchoke, K. Ryu, L. Gomez De Arco, A. Badmaev, C. Wang, C. Zhou, *Adv. Mater.* **2010**, *22*, 1900.
- [9] H. Jung, H. Lee, *Sens. Actuators, A* **2021**, *331*, 112876.
- [10] Y. Wang, L. Zhang, J. Zhou, A. Lu, *ACS Appl. Mater. Interfaces* **2020**, *12*, 7631.
- [11] S. Hozumi, S. Honda, T. Arie, S. Akita, K. Takei, *ACS Sens.* **2021**, *6*, 1918.
- [12] K. Xu, Y. Lu, K. Takei, K. Xu, Y. Lu, K. Takei, *Adv. Mater. Technol.* **2019**, *4*, 1800628.
- [13] Y. Lu, K. Xu, L. Zhang, M. Deguchi, H. Shishido, T. Arie, R. Pan, A. Hayashi, L. Shen, S. Akita, K. Takei, *ACS Nano* **2020**, *14*, 10966.
- [14] L. Lan, X. Le, H. Dong, J. Xie, Y. Ying, J. Ping, *Biosens. Bioelectron.* **2020**, *165*, 112360.
- [15] W. Jeong, J. Song, J. Bae, K. R. Nandanapalli, S. Lee, *ACS Appl. Mater. Interfaces* **2019**, *11*, 44758.
- [16] Y. Wang, S. Lee, T. Yokota, H. Wang, Z. Jiang, J. Wang, M. Koizumi, T. Someya, *Sci. Adv.* **2020**, *6*, 7043.
- [17] Y. Chen, B. Lu, Y. Chen, X. Feng, *Sci. Rep.* **2015**, *5*, 11505.
- [18] J. M. Tulliani, B. Inserra, D. Ziegler, *Micromachines* **2019**, *10*, 232.
- [19] Z. Wang, C. Zhao, T. Han, Y. Zhang, S. Liu, T. Fei, G. Lu, T. Zhang, *Sens. Actuators, B* **2017**, *242*, 269.
- [20] J. Cui, Y. Li, D. Chen, T.-G. Zhan, K.-D. Zhang, *Adv. Funct. Mater.* **2020**, *30*, 2005522.

- [21] M. Kar, O. Tutusaus, D. R. MacFarlane, R. Mohtadi, *Energy Environ. Sci.* **2019**, *12*, 566.
- [22] L. C. Fernandes, D. M. Correia, C. García-Astrain, N. Pereira, M. Tariq, J. M. S. S. Esperança, S. Lanceros-Méndez, *ACS Appl. Mater. Interfaces* **2019**, *11*, 20316.
- [23] Z. Lei, B. Chen, Y. M. Koo, D. R. Macfarlane, *Chem. Rev.* **2017**, *117*, 6633.
- [24] S. Zhang, S. Liu, Q. Zhang, Y. Deng, *Chem. Commun.* **2011**, *47*, 6641.
- [25] H. Ota, K. Chen, Y. Lin, D. Kiriya, H. Shiraki, Z. Yu, T. J. Ha, A. Javey, *Nat. Commun.* **2014**, *5*, 5032.
- [26] S. Xiao, J. Nie, R. Tan, X. Duan, J. Ma, Q. Li, T. Wang, *Mater. Chem. Front.* **2019**, *3*, 484.
- [27] T. Kozaki, S. Saito, Y. Otsuki, R. Matsuda, Y. Isoda, T. Endo, F. Nakamura, T. Araki, T. Furukawa, S. Maruo, M. Watanabe, K. Ueno, H. Ota, *Adv. Electron. Mater.* **2020**, *6*, 1901135.
- [28] J. Sun, G. Lu, J. Zhou, Y. Yuan, X. Zhu, J. Nie, *ACS Appl. Mater. Interfaces* **2020**, *12*, 14272.
- [29] X. Zhao, K. Zhou, Y. Zhong, P. Liu, Z. Li, J. Pan, Y. Long, M. Huang, A. Brakat, H. Zhu, *Nano Res.* **2021**, *14*, 1202.
- [30] Y. Lin, E. Bilotti, C. W. M. Bastiaansen, T. Peijs, *Polym. Eng. Sci.* **2020**, *60*, 2351.
- [31] S. Caimi, H. Wu, M. Morbidelli, *ACS Appl. Energy Mater.* **2018**, *1*, 5224.
- [32] M. Li, X. Zhang, S. Zeng, L. Bai, H. Gao, J. Deng, Q. Yang, S. Zhang, *RSC Adv.* **2017**, *7*, 6422.
- [33] L. Pedersen, G. B. E. Jemec, *Acta Derm.-Venereol.* **2006**, *86*, 308.
- [34] S. Luebberding, N. Krueger, M. Kerscher, *Int. J. Cosmet. Sci.* **2013**, *35*, 477.
- [35] K. Prasad, M. Nikzad, I. Sbarski, *J. Polym. Res.* **2018**, *25*, 232.
- [36] J. Leys, R. N. Rajesh, P. C. Menon, C. Glorieux, S. Longuemart, P. Nockemann, M. Pellens, K. Binnemans, *J. Chem. Phys.* **2010**, *133*.
- [37] I. You, D. G. MacKanic, N. Matsuhisa, J. Kang, J. Kwon, L. Beker, J. Mun, W. Suh, T. Y. Kim, J. B. H. Tok, Z. Bao, U. Jeong, *Science* **2020**, *370*, 961.
- [38] H. Farahani, R. Wagiran, M. N. Hamidon, *Sensors (Basel)*. **2014**, *14*, 7881.
- [39] K. R. Seddon, A. Stark, M. J. Torres, *Pure Appl. Chem.* **2000**, *72*, 2275.
- [40] H. Yeon, H. Lee, Y. Kim, D. Lee, Y. Lee, J. S. Lee, J. Shin, C. Choi, J. H. Kang, J. M. Suh, H. Kim, H. S. Kum, J. Lee, D. Kim, K. Ko, B. S. Ma, P. Lin, S. Han, S. Kim, S. H. Bae, T. S. Kim, M. C. Park, Y. C. Joo, E. Kim, J. Han, J. Kim, *Sci. Adv.* **2021**, *7*, eabg8459.
- [41] D. H. Ho, Q. Sun, S. Y. Kim, J. T. Han, D. H. Kim, J. H. Cho, *Adv. Mater.* **2016**, *28*, 2601.

ADVANCED MATERIALS TECHNOLOGIES

Supporting Information

for *Adv. Mater. Technol.*, DOI: 10.1002/admt.202200209

Transparent and Breathable Ion Gel-Based Sensors
toward Multimodal Sensing Ability

*Yuji Isano, Hajime Fujita, Koki Murakami, Sijie Ni, Yuta Kurotaki, Tamami Takano, Yutaka Isoda, Ryosuke Matsuda, Fumika Nakamura, Yuuki Nishitai, Nyamjargal Ochirkhuyag, Kota Inoue, Hiroki Kawakami, Yusuke Okubo, Kazuhide Ueno, Toshinori Fujie, and Hiroki Ota**

Supporting Information

Transparent and Breathable Ion Gel-based Sensors towards Multimodal Sensing Ability

Yuji Isano ^a, Hajime Fujita ^b, Koki Murakami ^a, Sijie Ni ^a, Yuta Kurotaki ^a, Tamami Takano ^a, Yutaka Isoda ^a, Ryosuke Matsuda ^a, Fumika Nakamura ^a, Yuuki Nishitai ^a, Nyamjargal Ochirkhuyag ^a, Kota Inoue ^a, Hiroki Kawakami ^a, Yusuke Okubo ^c, Kazuhide Ueno ^{d,e}, Toshinori Fujie ^b, and Hiroki Ota* ^{a,f}

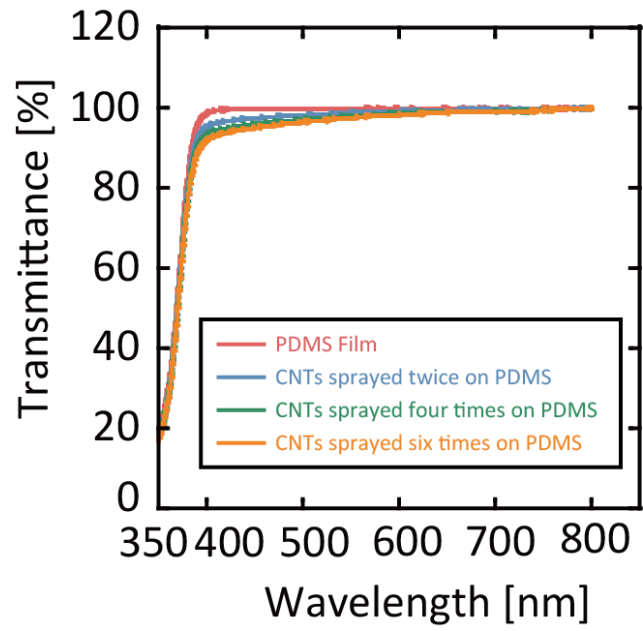


Figure S1. Light transmission spectra of the PDMS substrate sprayed with only CNTs for varying number of CNT sprays.

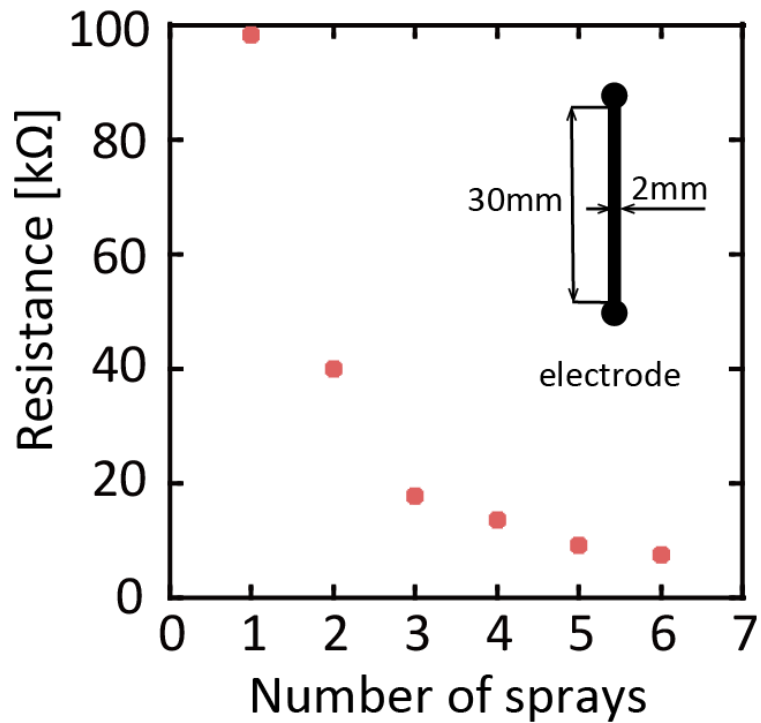


Figure S2. Relationship between the resistance change in CNT electrodes sprayed with a homemade spray coater and the number of sprays. The inset schematic shows the geometry of the electrodes used in the test.

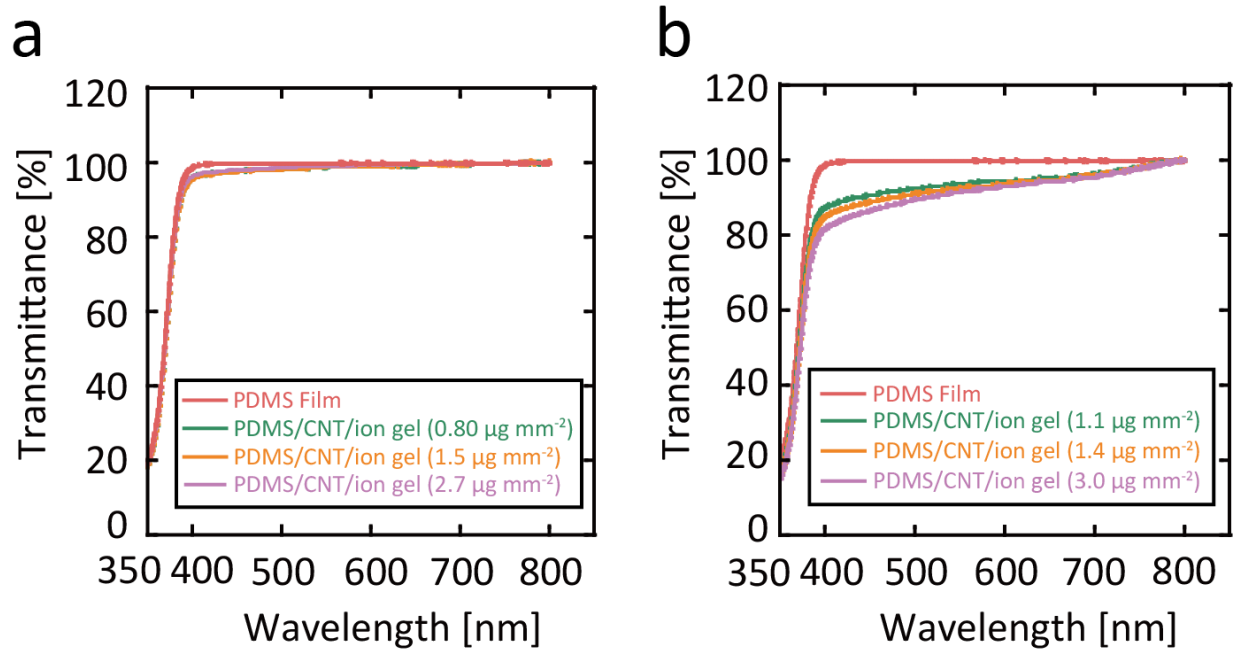
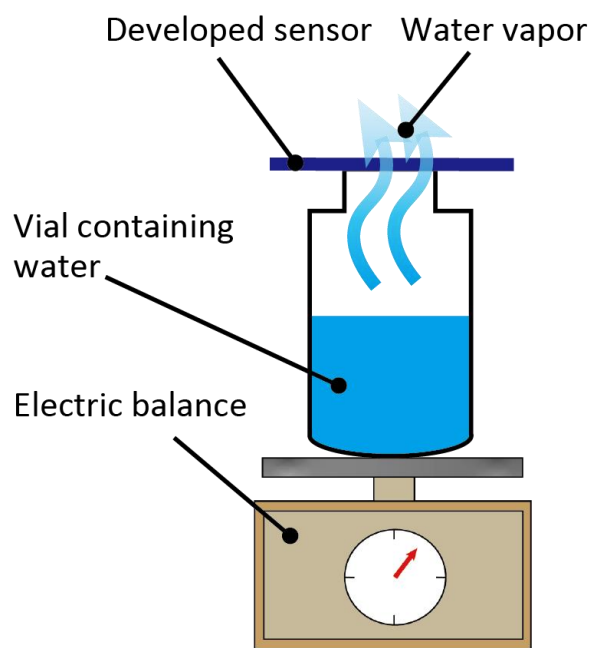


Figure S3. Light transmission spectra according to the mass per unit area of sprayed (a) hydrophilic and (b) hydrophobic ion gel. The PDMS substrate was coated with CNTs four times.

a



b

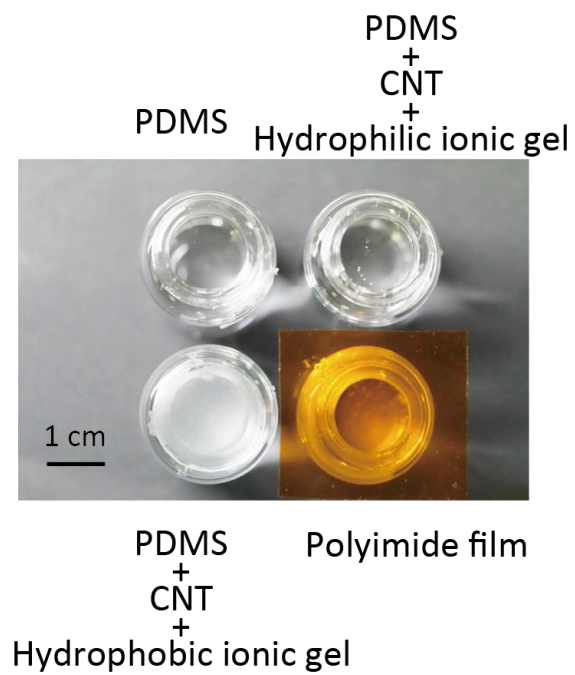


Figure S4. Moisture permeability tests: (a) Schematic representation of the experiment; (b) Vials sealed with various films used in the experiments.

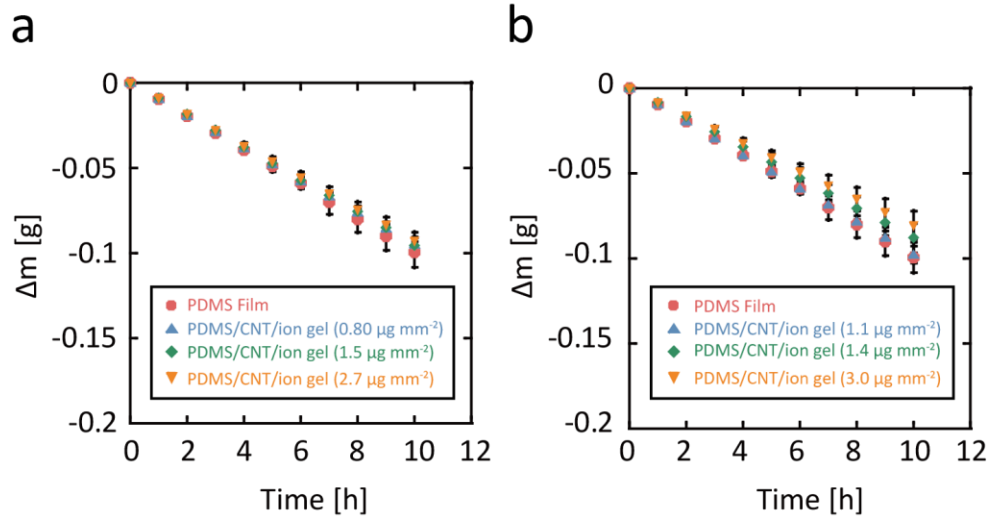


Figure S5. Moisture permeation with respect to the mass per unit area of sprayed (a) hydrophilic and (b) hydrophobic ion gels; $n = 8$ for $0.80 \mu\text{g mm}^{-2}$ and $1.5 \mu\text{g mm}^{-2}$ hydrophilic ion gel, $n=9$ for the other samples. The PDMS substrate was coated with CNTs four times. The data is shown by mean \pm standard deviation.

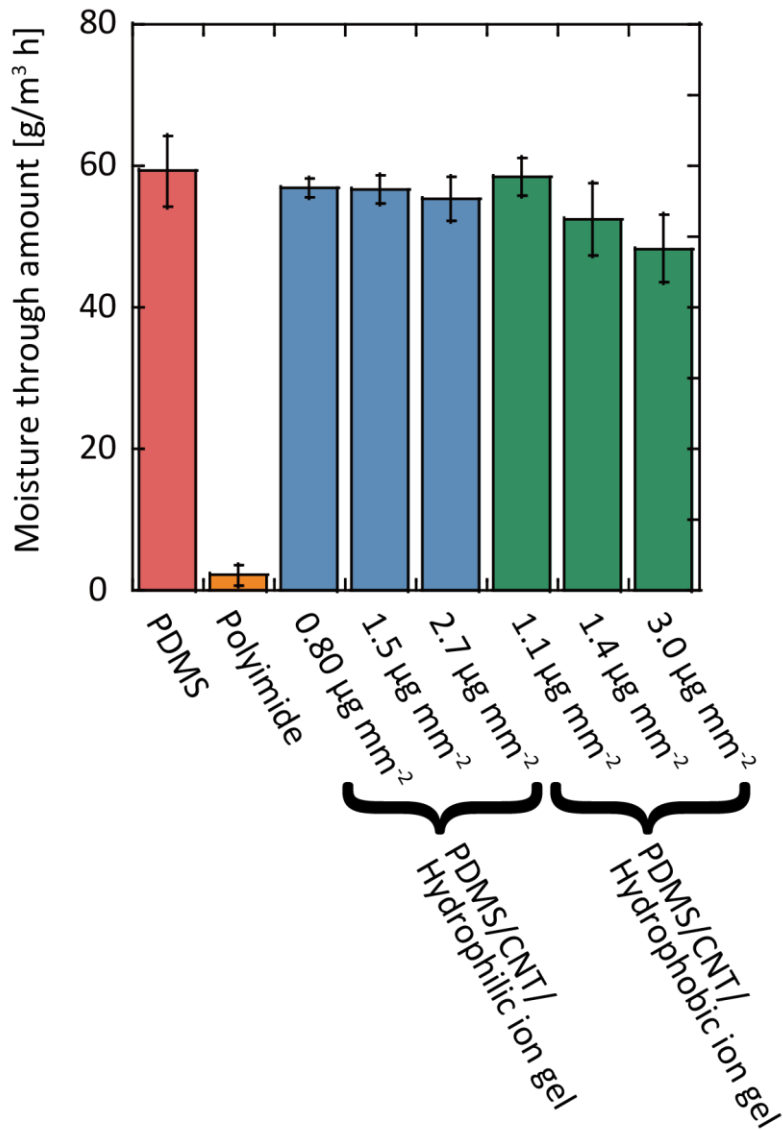


Figure S6. Results of repeated tests of water vapor transmission of the film; n = 8 for 0.80 µg mm⁻² and 1.5 µg mm⁻² hydrophilic ion gel, n=9 for the other samples. The data is shown by mean ± standard deviation.

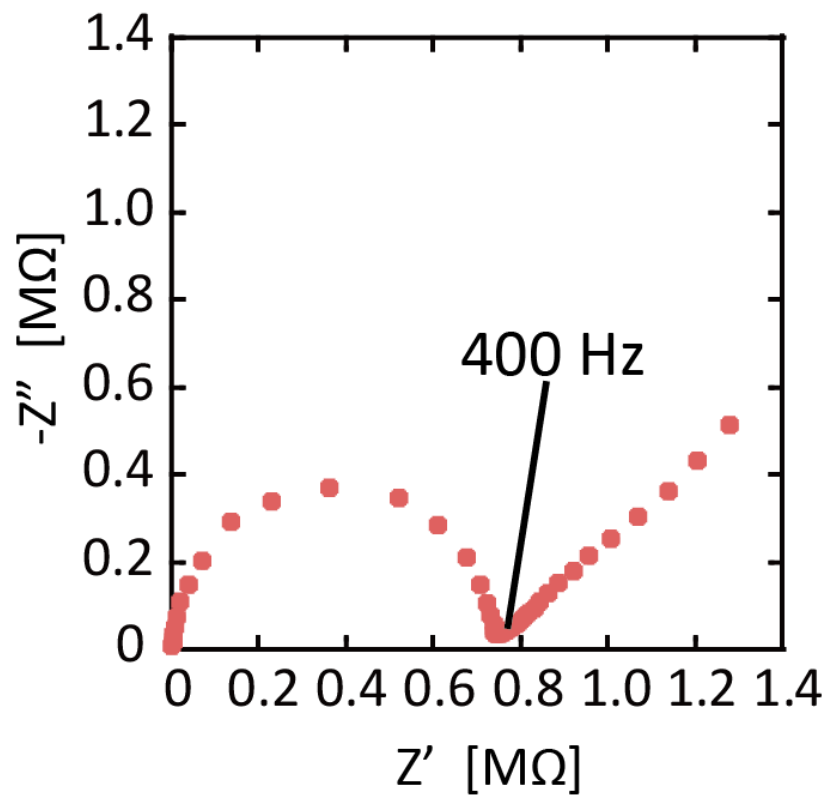


Figure S7. Nyquist plot of hydrophilic ion gel at 30 °C and 50% RH. The sensor measurement was performed at 400 Hz.

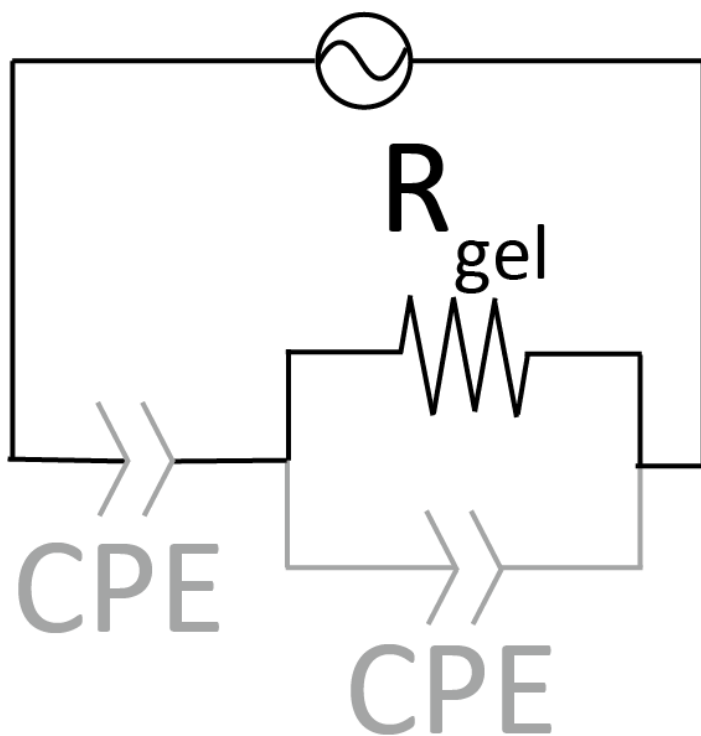


Figure S8. Equivalent circuit of the developed ion gel-based sensor. The gray-colored part corresponds to the imaginary portion of the impedance, and it is almost negligible at this frequency. Because the capacitance component of the ion gel is neglected, ion transfer is the dominant factor in the measured impedance.

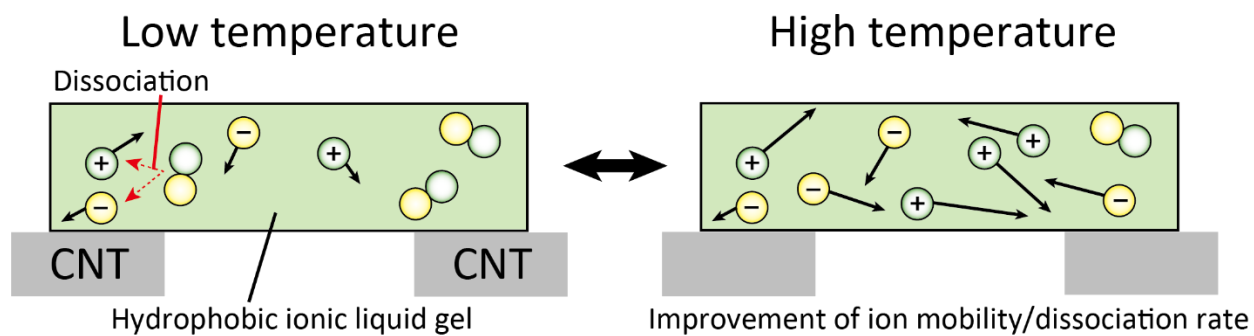


Figure S9. Temperature sensing principle of the developed sensor.

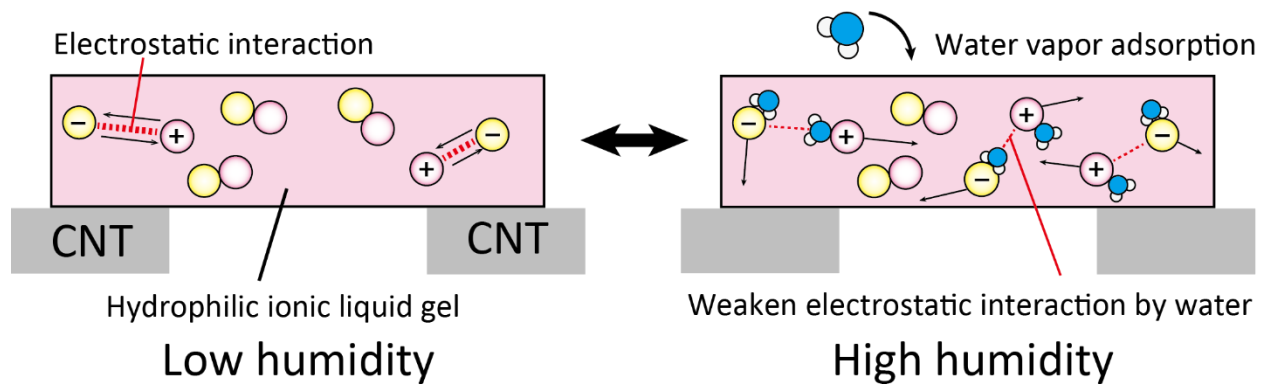


Figure S10. Humidity sensing principle of the developed sensor.

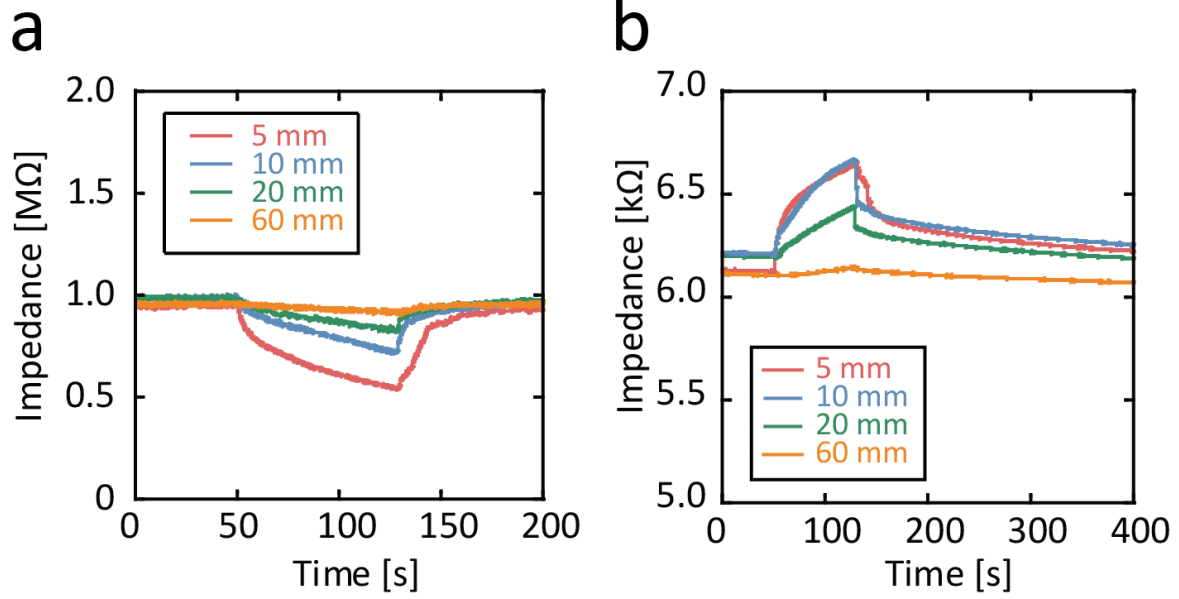


Figure S11. Impedance changes in the sensors when compared to the ion gel humidity sensor during proximity sensing. (a) Ion gel temperature sensor; (b) CNT humidity sensor.

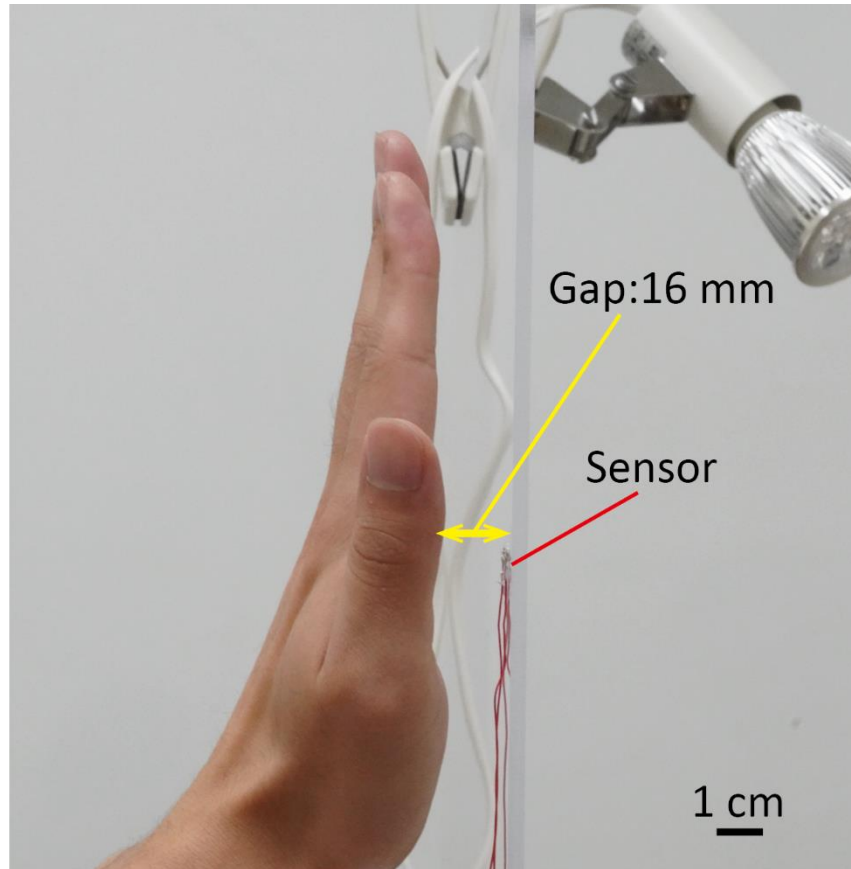


Figure S12. Magnified cross-sectional view of the proximity switching demonstration. The distance between the sensor and the hand is approximately 16 mm.

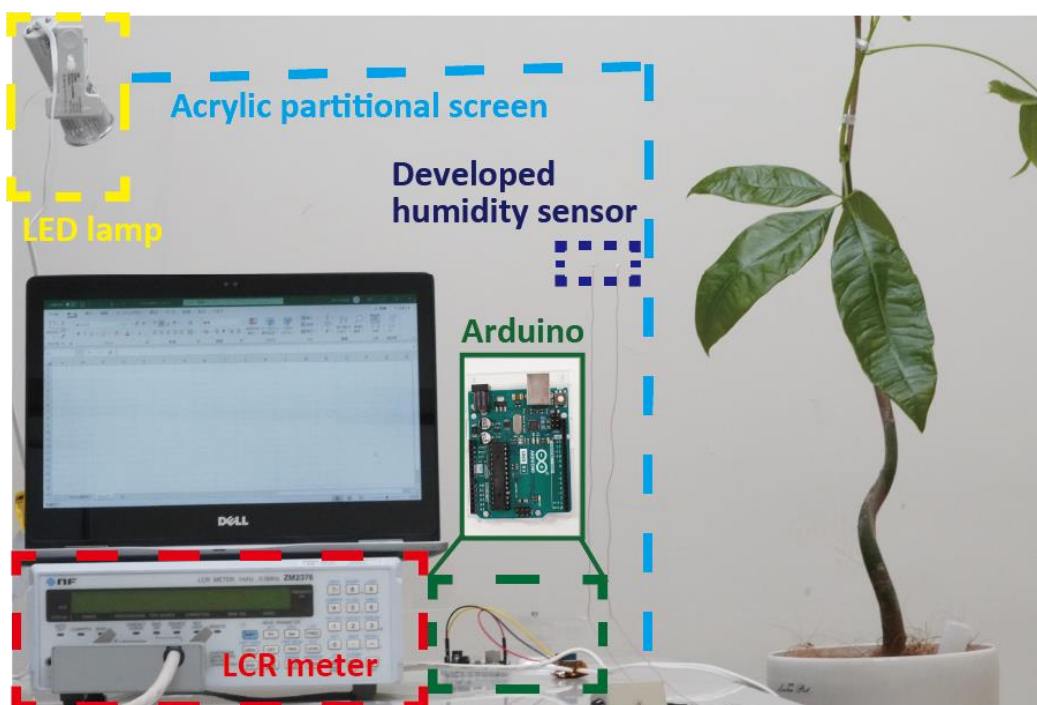


Figure S13. Experimental system for proximity switching demonstration.

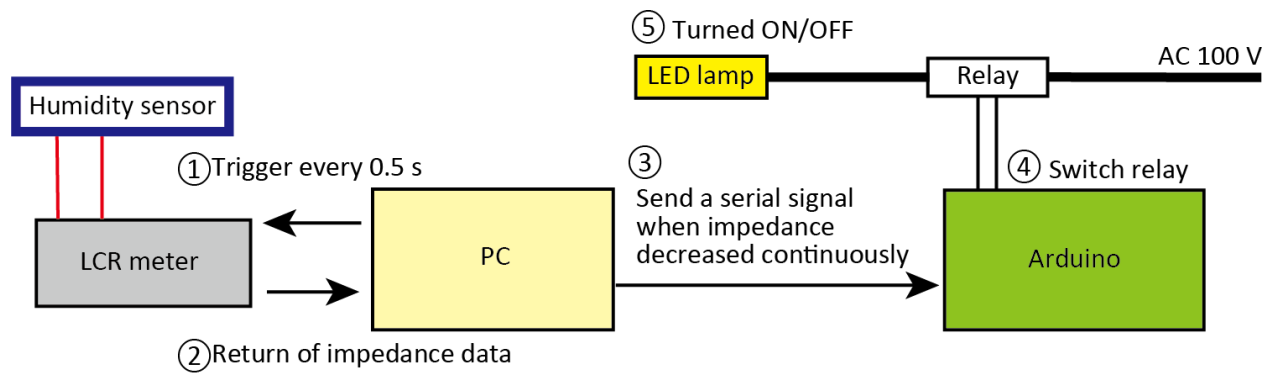


Figure S14. Schematic of the proximity switching demonstration. The measurement results are processed by a PC, and a signal from the PC, which is triggered by a continuous drop in impedance, controls the Arduino to turn the relay on and off.

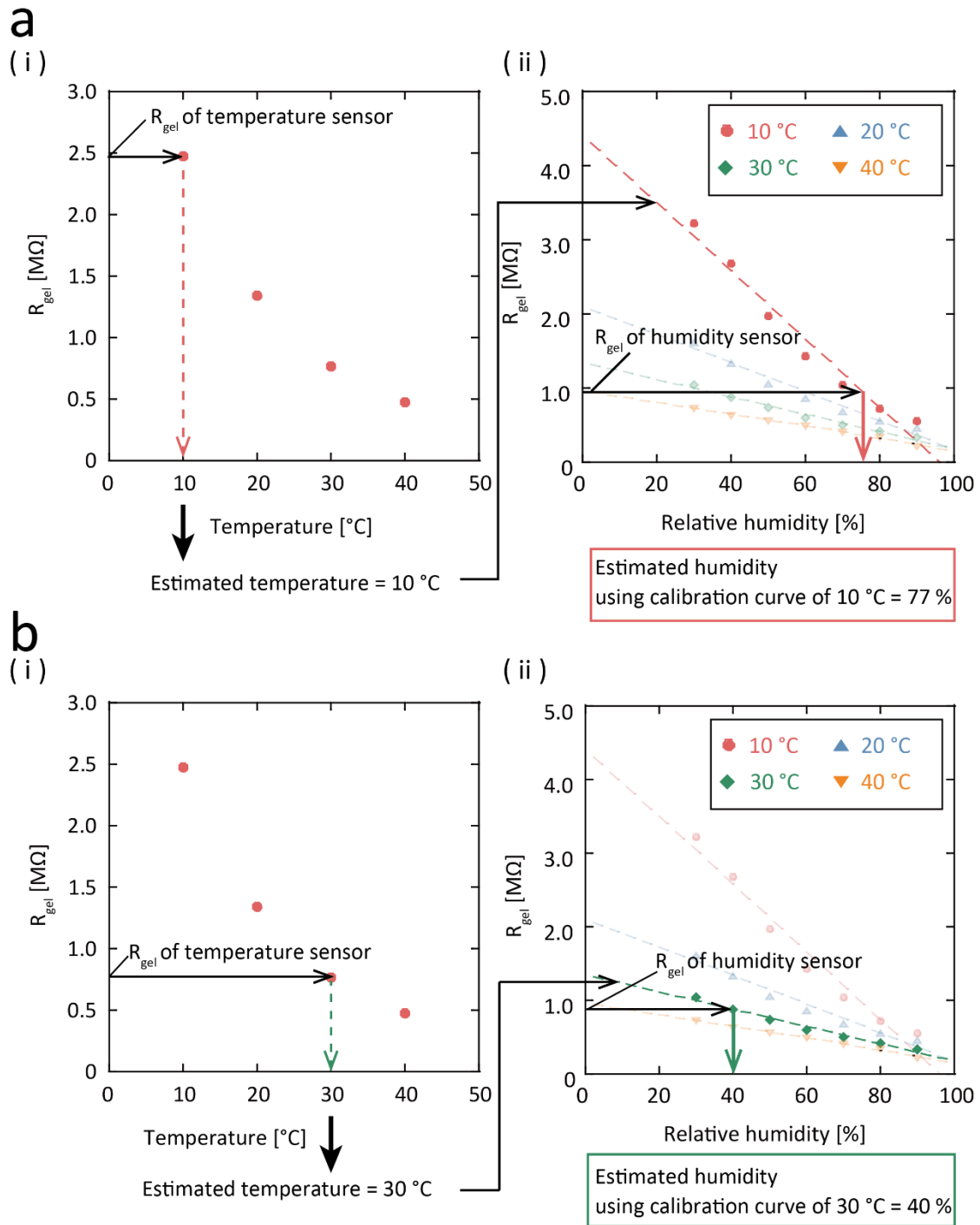
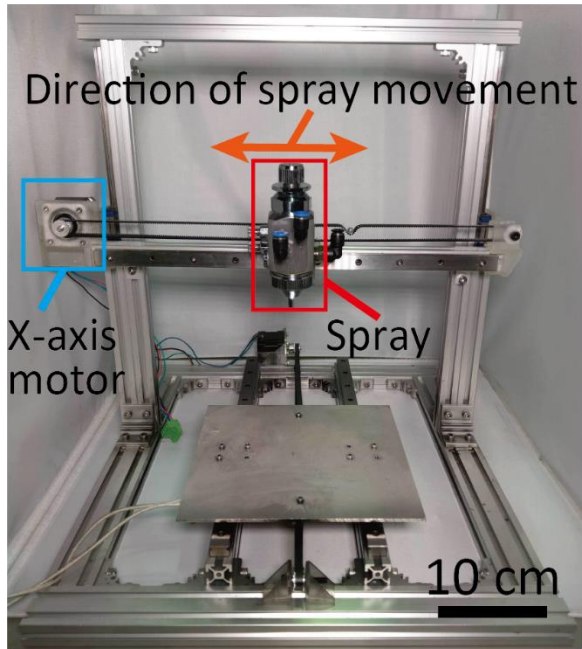
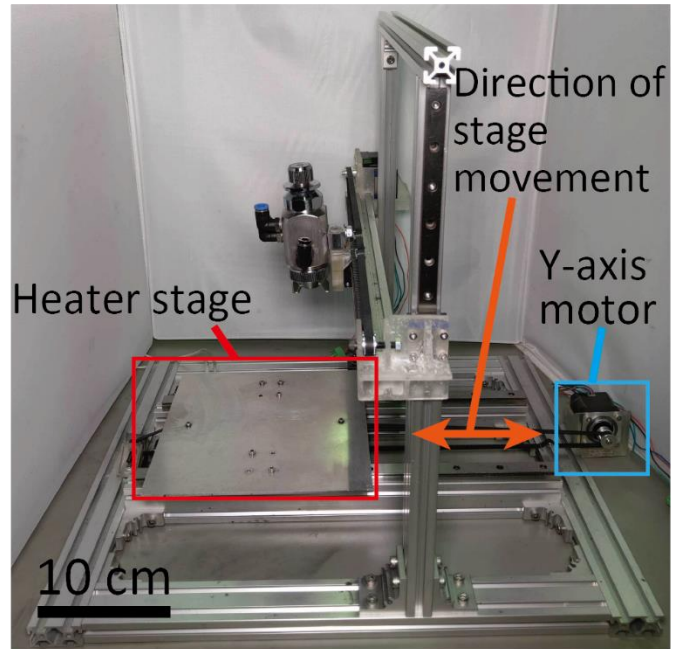


Figure S15. Schematic diagrams of the compensation of the developed humidity sensor using the temperature sensor at 10 °C and 30 °C. The humidity sensor estimates the temperature from the output value of the temperature sensor and determines the calibration curve used for the R_{gel} .humidity conversion of the humidity sensor. Example of the correction at (a) 10 °C and (b) 30 °C.



Front view



Side view

Figure S16. Front and side views of the developed spray coater.

Table S1: Variation in the ion gel mass, light permeability, water vapor permeability, linearity, and sensitivity of the humidity sensor with the spray time of the hydrophilic ion gels

Spray time [s]	Ion gel mass [$\mu\text{g mm}^{-2}$]	Transmittance [%]	Water vapor permeability [$\text{g m}^{-2} \text{h}^{-1}$]	Linearity R^2	Sensitivity [% per RH%]
2	-	99	-	Not worked	Not worked
6	0.80	99	57	0.948	2.0
10	1.5	99	57	0.988	1.7
20	2.7	99	55	0.949	1.6

Table S2: Ion gel mass, light transmission, water vapor transmission, and temperature sensor error ranges with humidity as a function of the spray time when spray coating the hydrophobic ion gels

Spray time [s]	Ion gel mass [$\mu\text{g mm}^{-2}$]	Transmittance [%]	Water vapor permeability [$\text{g m}^{-2}\text{h}^{-1}$]	Error ranges with humidity at 20 °C
2	-	93	-	Not worked
6	1.1	94	58	± 7.3 %
10	1.4	93	52	± 6.4 %
20	3.0	91	49	± 5.1 %

Table S3. Comparison of the proposed humidity sensor with other published works

Ref	Materials/Electrodes/Substrate	Output type	Tested RH range	Response/Recovery Time	Linearity	Visible light transmittance	Flexible	Gas Permeability	Temperature dependency
Ho et al. ^[1] Wu et al. ^[2]	GO/graphene/PDMS	C	20%–90%	~200/150 [s]	No	90%	Yes	NA	Independent
Wang et al. ^[3]	Cellulose + KOH Freestanding film	R	11.3%–97.3%	6.0/10.8 [s]	No	87.14% at 550 [nm]	Yes	NA	Independent
Luo et al. ^[4]	Silk fibroin/AgNW/PET film	C	40%–95%	Can detect 4 [Hz] humidity change	Yes	87.1% at 520 [nm]	Yes	NA	NA
Zhao et al. ^[5]	PVDF-HFP+[EMIM][BF ₄] Freestanding film	Z	10%–80%	Can detect 30 [Hz] humidity change	Yes	93%	Yes	NA	NA
Trung et al. ^[6]	rGO+PU/PEDOT:PSS+PU/PDMS	R	10%–70%	3.5/7.0 [s]	Yes	78% (average in visible area)	Yes	NA	NA
Jeong et al. ^[7]	PVA + Parylene + Au nanomesh	R	25%–98%	148/110 [s]	No	NA	Yes	Yes	Not independent
This work	[Li(G4)] [TFSA]+Pebax1657/ CNT/PDMS	Z	30%–90%	6.2/49.9 [s]	Yes	99% at 550 [nm]	Yes	58.7 [g/m ² h]	With temperature compensation

* R: resistance, C: capacitance, Z: impedance, GO: graphene oxide, rGO: reduced graphene oxide, PET: polyethylene terephthalate, [EMIM][BF₄]: 1-ethyl-3-methylimidazolium tetrafluoroborate, PEDOT:PSS: (3, 4-ethylenedioxythiophene) poly(styrene sulfonate), PU: polyurethane

References

- [1] D. H. Ho, Q. Sun, S. Y. Kim, J. T. Han, D. H. Kim, J. H. Cho, *Adv. Mater.* **2016**, *28*, 2601.
- [2] J. Wu, Z. Wu, H. Xu, Q. Wu, C. Liu, B. R. Yang, X. Gui, X. Xie, K. Tao, Y. Shen, J. Miao, L. K. Norford, *Mater. Horizons* **2019**, *6* (3), 595.
- [3] Y. Wang, L. Zhang, J. Zhou, A. Lu, *ACS Appl. Mater. Interfaces* **2020**, *12* (6), 7631.
- [4] Y. Luo, Y. Pei, X. Feng, H. Zhang, B. Lu, L. Wang, *Mater. Lett.* **2020**, *260*, 126945.
- [5] X. Zhao, K. Zhou, Y. Zhong, P. Liu, Z. Li, J. Pan, Y. Long, M. Huang, A. Brakat, H. Zhu, *Nano Res.* **2021**, *14* (4), 1202.
- [6] T. Q. Trung, L. T. Duy, S. Ramasundaram, N. E. Lee, *Nano Res.* **2017**, *10* (6), 2021.
- [7] W. Jeong, J. Song, J. Bae, K. R. Nandanapalli, S. Lee, *ACS Appl. Mater. Interfaces* **2019**, *11*, 47, 44758.